EXPERIMENTAL DESIGN AND FLOW VISUALIZATION FOR THE UPPER PLENUM OF A VERY HIGH TEMPERATURE GAS COOLED FOR COMPUTER FLUID DYNAMICS VALIDATION

A Thesis

by

KYLE LEROY MCVAY

Submitted to the Office of Graduate and Professional Studies of
Texas A&M University
in partial fulfillment of the requirements for the degree of

MASTER OF SCIENCE

Chair of Committee,	Nagamangala Anand
Co- Chair of Committee,	Yassin Hassan
Committee Members,	Hamn Chen
	Sai Lau
Head of Department,	Andreas Polycarpou

August 2014

Major Subject: Mechanical Engineering

ABSTRACT

The Very High Temperature Reactor (VHTR) is a Generation IV nuclear reactor that is currently under design. It modifies the current high temperature gas reactor (HTGR) design to have a 1000 ^{0}C coolant outlet. This increases fuel efficiency and allows for other industrial applications. During the design process several studies are performed to develop safety codes for the reactor. One major accident of interest is the Pressurized Conduction Cooldown (PCC) scenario. The PCC scenario involves loss of forced coolant to the core but the loop stays pressurized. This results in a large buoyancy force that through natural convection reverses the flow of the core coolant loop to circulate into the upper plenum of the VHTR. Computer codes may be developed to simulate the phenomenon that occurs in a PCC scenario, but benchmark data is needed to validate the simulations. There are currently no experimental models to provide benchmark data for the PCC scenario. This study will cover the design, construction, and testing of a 1/16th scaled model of a VHTR that uses Particle Image Velocimetry (PIV) for flow visualization in the upper plenum. Three tests were run for a partially heated core at statistically steady state, and PIV was used to generate the velocity field of three naturally convective adjacent jets. Recirculation between the jets occurred until the jets reached the mixing point three cm from the outlet where turbulent mixing was observed. A sensitivity analysis was performed to confirm 1000 image pairs was sufficient to correctly represent the flow. The results were then validated by comparing the PIV results with experimental data and calculated values.

ACKNOWLEDGEMENTS

First I would like to thank the Department of Energy for funding this project. I am honored for the opportunity to work on such exciting and stimulating research. I'd also like to thank Dr. Richard Schultz and everyone else at Idaho National Laboratories for their research and work in organizing this project.

I would like to thank Dr. Yassin Hassan and Dr. N.K. Anand who were great advisors despite their busy schedules. Researching under such experienced and respected advisors has been a gift, and I am grateful for the guidance as well as the freedom given while performing my research.

My sincere thanks go to my colleague Saya Lee. His experience and knowledge was crucial for this study. He had an answer to my every question and problem, and was usually correct. I'd also like to thank Robert Park my research partner and friend, who acted as my counterbalance and was enjoyable to work with. Likewise I'd like to thank my labmate Pratanu Roy, who I could always count on for sensible professional advice.

Finally I would like to thank my parents who raised me with the morals to become who I am today, and who have supported me throughout my academic career. I wouldn't be an engineer today without you.

TABLE OF CONTENTS

Page

LIST OF FIGURES

Page

1 INTRODUCTION

The world is ever growing, and the energy demands grow with it. The United States energy consumption from just 2010 to 2013 has grown from 74.769 to 81.664 Quadrillion Btu, a 9% increase and 78% of the energy consumed in 2013 were fossil fuels[1]. As the fossil fuels grow scarcer and the demand for alternative energy rises the nuclear industry will continue to develop to meet this demand and with it the safety codes governing them. Intensive safety analysis has been performed for currently operating reactors, and several safety systems are employed to ensure safe operation and that the correct procedures are taken in case of emergency conditions to minimize further damage. Older reactor models safety systems rely on pumps, electricity, and human interaction all of which may fail resulting in serious damages to human health, the reputation of the nuclear industry, and monetary loss. In light of this the current Gen III reactors, such as the AP1000 developed by Westinghouse, employ passive safety systems. Instead of using active components, passive safety systems use natural forces such as gravity, pressure, and compressed gases to keep the core and containment from overheating and melting the fuel for an extended period of time [2]. As the industry advances into the next generation of reactors, the safety systems must evolve with it.

1.1 Project Background

The Very-high-temperature-reactor (VHTR) is a prominent Generation IV nuclear reactor design. The VHTR loosely includes any reactor design with a coolant outlet temperature about 1000 ^{0}C or above[3]. However it is typically used when

discussing the evolutionary development of the high-temperature gas-cooled reactors (HTGR). The HTGR is largely defined by its fuel design. The fuel is comprised of small particles that are coated with porous graphite, layers of pyrolytic carbon, silicon, and carbide. These particles are then loaded into several spheres and are grouped in the core, or the fuel is loaded into thin rods and arranged in a hexagonal pattern following the prismatic design[4]. The fuel particles can withstand very high temperatures and will not fail below 1600 ^{0}C permitting the design of the HTGR. The current HTGRs in operation operate with an outlet of 850 ^{0}C, where employing the VHTR technology design would increase the outlet temperature to 1000 ^{0}C or greater.

Because of the high outlet temperature the VHTR enables it for other applications besides energy production. One application is the mass production of hydrogen. As efficient fuel cells are developed and the demand for hydrogen grows a new market based on hydrogen power is introduced. Currently 95% of the hydrogen being produced uses valuable natural gases, which makes is economically unusable for consumer use[5]. A more environmentally friendly and economically viable production of hydrogen would use a nuclear energy system to mass produce the hydrogen. The hot steam produced by nuclear reactors, particularly the VHTR, is optimal for electrolysis in hydrogen production. Said hydrogen could be used to replace fossil fuels in multiple applications such as automobiles[6]. Another application of the VHTR is heat production to be used in industrial applications such as coal gasification or petrochemical operations. The VHTR is designed to have high fuel efficiency and maintain the safety characteristics of the modular high temperature gas-cooled reactors.

Studies by Idaho National Engineering and Environmental Laboratory (INEEL) on a pebble bed and prismatic design for the HTGR shows that both of their designs meet the three basic requirements set for the Next Generation Nuclear Plant (NGNP): a coolant outlet of 1000 ^{0}C, passive safety systems, and a total power output that meets the expected output for commercial HTGR, making the VHTR design the leading candidate for the NGNP and a prominent focus for studies[5].

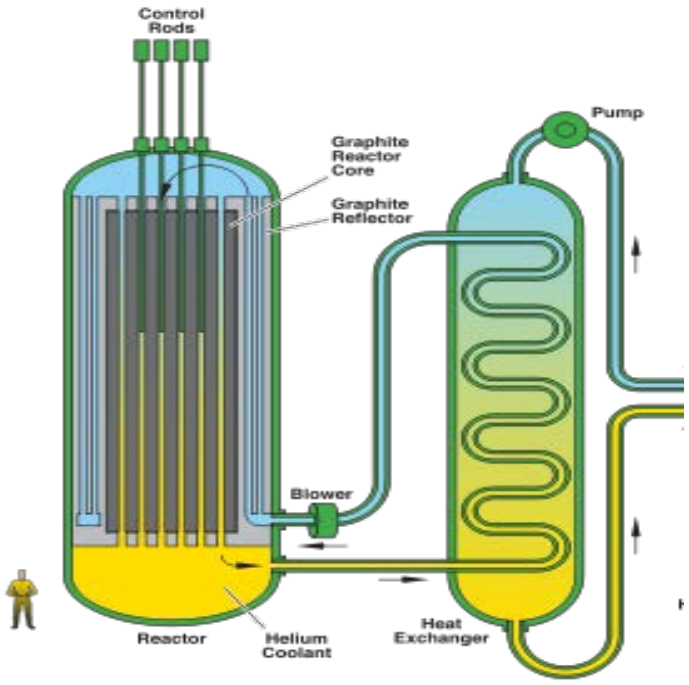

Figure 1-1:VHTR under normal operation

Since the VHTR is still in design phase, multiple studies are being performed that can be used in developing the safety codes. Multiple accident scenarios as well as normal operation are of interest. Two primary accident scenarios for the VHTR are the Pressurized Conduction Cooldown (PCC) and the Depressurized Conduction Cooldown

(DCC). Under normal operation a blower is used to pump the coolant up between the reflector and the core, where it then impinges on the upper plenum and goes down through the core as seen in Figure 1-1, resulting in forced convection for core cooling[7]. A PCC scenario occurs most commonly during a loss of power scenario. The blower fails and the forced convection fails with it. Because the loop is still pressurized the gas density remains high which leads to a large buoyancy force. Over time this force reverses circulation through the core, causing the coolant, normally helium, to rise from the lower plenum up through the core, into the upper plenum, and down between the reflector and the core. The DCC scenario occurs when the main pressure loop has been breached. Hot helium is vented out and cold air ingress floods the containment. Because the containment is depressurized the buoyancy force is insufficient to counteract the inertial forces. This causes the cold air to pool at the bottom of the containment where it eventually diffuses through the hot coolant, usually helium. This process can be seen in Figure 1-2[8]. This is much slower than the PCC scenario's buoyancy driven, making the DCC scenario more critical as the core will reach higher temperatures.

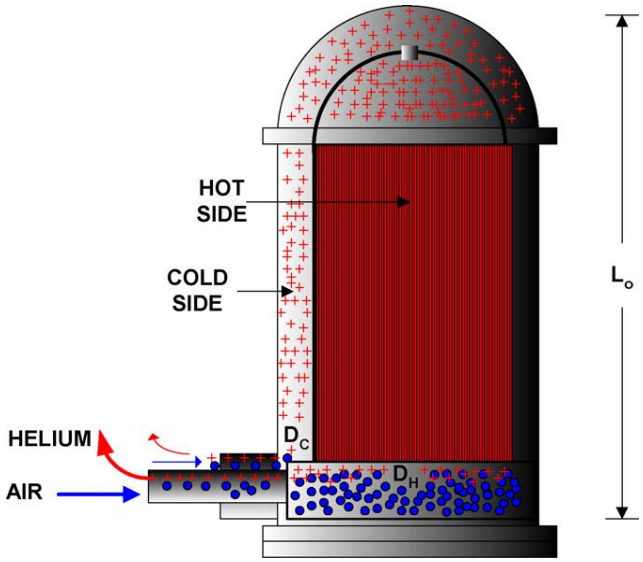

Figure 1-2: Air ingress causing DCC scenario for a VHTR

1.2 Research Objectives

The primary focus of this study is the design, construction, and testing of a scaled ($1/16^{th}$) experimental facility that models a VHTR. The model must be able to extract data relating to flow visualization and other thermal hydraulic phenomena in the upper plenum and be used to validate Computer Fluid Dynamics (CFD) codes.

The design of this facility accounted for several parameters which include: the scaled geometry from INL, fabrication process limitations, can supply sufficient heat to the modeled core for testing, a heat sink sufficient to remove the heat input, and a system that allows for sufficient data acquisition. Once this facility was designed and constructed, the testing may begin.

The experimental facility uses Particle Image Velocimetry (PIV) to measure the velocity field of a planar cross section in the upper plenum of the scaled model. This study obtains particle images that are processed using PIV techniques, and the results are

validated. First a sensitivity analysis is performed to determine the sufficient number of images to correctly represent the flow field. Then multiple tests are compared to each other for repeatability. Finally the PIV results are validated by comparing them with an ultrasonic flowmeter and calculated flowrates.

1.3 Outline

This chapter describes the Background and Validation for this study. It largely focuses on the design and future applications of the VHTR, as well as the accident scenarios of interest. It also covers the objectives for this study.

Chapter 2 will provide information performed in previous studies performed related to the VHTR. Additionally it will go over the scaling and modeling performed in other studies that relate to the test facility.

Chapter 3 will explain the procedure in designing the experimental test facility. It will also cover the assembly process after the parts are finished machining and problems encountered, as well as the data acquisition layout and parts selection.

Chapter 4 will cover the testing procedure, data analysis, and the results. Additionally an example computer fluid dynamics simulation is discussed.

Chapter 5 has the conclusion which provides a summary and what has been gained from the study, as well as future possible work that can be accomplished with the test facility.

2 LITERATURE REVIEW

2.1 Previous Studies - Simulations

A transient numerical model was used by Haque to simulate the flow through the core after the accident occurs[9]. The temperature profile can be seen below in Figure 2-1 and the temperature profile in Figure 2-2. Their thermal hydraulic code THERMIX has been verified with experimental data[10]. Initially the hottest part of the core is in the lower half, but as the buoyancy forces overpower the inertial forces, the flow reverses and the temperature profile shifts towards the top of the core. This study also evaluated a DCC scenario. Without the natural circulation the corereached 1587 ^{0}C, near the failing point of the fuel. Because the DCC scenario is more severe there has been more research on the behavior of the system following depressurization.

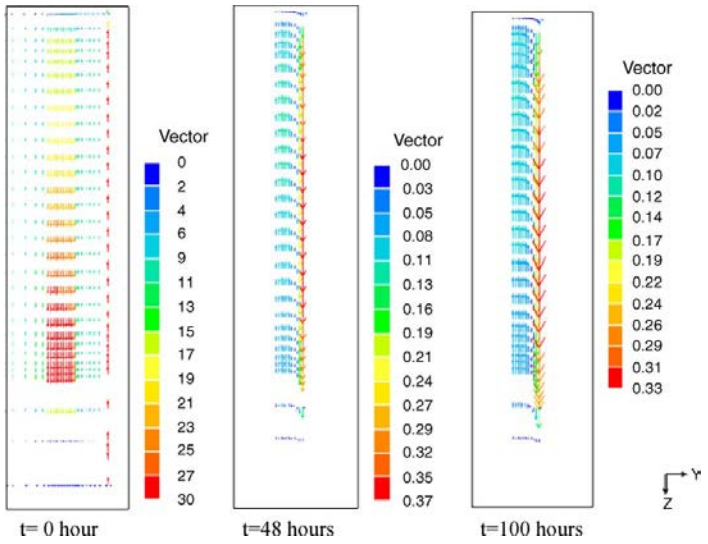

Figure 2-1: VHTR velocity profile following a PCC accident scenario

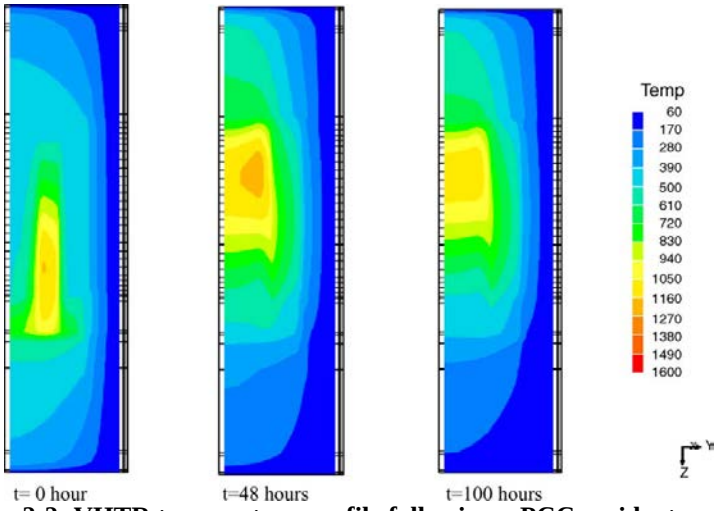

Figure 2-2: VHTR temperature profile following a PCC accident scenario

Tung and Johnson working with INL published a study in 2011 of CFD analysis for a 1/12th sector of a heated column of prismatic blocks that covers the heated portion of the core of a prismatic VHTR[11]. Using the steady state operating conditions as the initial conditions, Star-ccm+ was used for a transient analysis following a PCC scenario. Their mesh used 7.6 million cells for the core, and a total of 11.1 million cells with the upper and lower plenum. Figure 2-3 shows the velocity contour at the top of the core. Buoyancy forces drive the flow up through the center of the core as its hotter there, and then because there is no outlet for their model it goes down the coolant channels at the edge. They claim that though in reality there is an outlet, the flow resistance to go to the outlet and down to the lower plenum is higher than the nearby coolant channels, so the down-flow should occur in exterior coolant channels. Figure 2-4 shows the flow streamlines in the upper plenum. The flow impinges onto the top of the upper plenum, which is flat and doesn't represent the geometry of the actual VHTR.

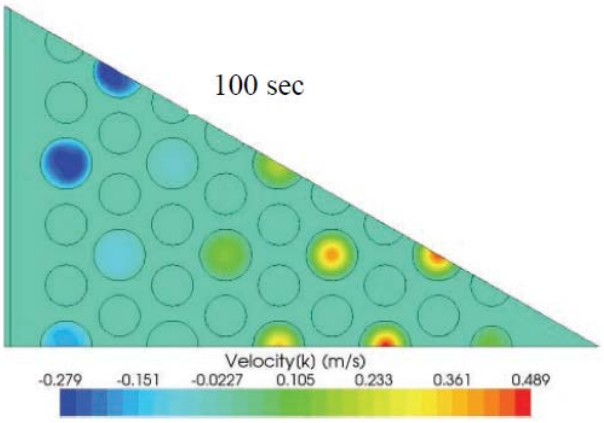

Figure 2-3: Velocity contour at top of the VHTR core 100 seconds after PCC scenario

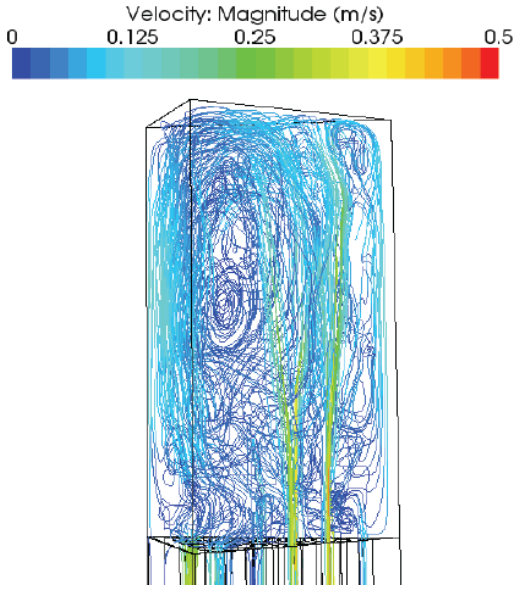

Figure 2-4: Streamline plot of the upper plenum 100 seconds after the PCC scenario

The French CEA released a study in 2002 about the thermal fluctuations in the lower plenum of a HTGR[12]. There are internal structures below the reactor that are important in supporting the core. Part of this structure is subjected to 850^0C helium near the outlet, but also subjected on its other side to 450^0C helium coming from the cold duct resulting in a sharp temperature gradient. Because of this their study focused on estimating the thermal stresses induced by the temperature gradient in the different support structures, which requires thermal and flow analysis in the lower plenum. They used the CATHARE code to perform global simulations which gave accurate boundary conditions[13]. These conditions were then used for transient CFD simulations for 4.5 seconds. Their results analyzed the oscillating characteristics and the mixing of flows that occurs.

Idaho National Laboratories (INL) has performed significant analysis for normal operations, DCC scenario, and partial loss of active coolant. INL has worked with the Korea Advanced Institute of Technology (KAIST), Seoul National University (SNU), and the University of Michigan (UM) to develop safety codes for the VHTR [14]. In March 2006 INL submitted a report to the Department of Energy (DOE) their study which focused on a loss-of-coolant accident (LOCA) resulting in a DCC scenario. LOCA accidents can lead to significant fuel damage of a VHTR. The tests modeled a new reactor core cooling system (RCCS) that used water instead of air as the coolant, and removed complex structures of other currently used water cooled RCCS models. Three scenarios were tested: normal operation, partial active cooling failure, and a loss of coolant (LOCA) scenario. To model this, an intensive CFD code was developed by KAIST to model the thermo-fluid phenomena that occurs in the multi-component mixture when an air and water ingress accident occurs in a VHTR. Two experiments were used to validate the code. A water pool reactor core cooling system (RCCS) was built at SNU, and an inverse U-tube experiment that predicted the thermo-fluid and chemical reaction behavior of a multi-component mixture. The codes were developed, refined, and validated with experimental measurements to be used in calculations for safety issues during a DCC accident in a VHTR, normal operations, and partial failure of active coolant.

2.2 Previous Studies – Scaling and Modeling

In September 2006 INL submitted a report to the Department Of Energy (DOE) for the experimental modeling of a VHTR during normal operation and a PCC scenario[15]. A lower plenum model would be used to model hot streaking and thermal striping phenomena that occurs during normal operation. Another model would be needed to model the upper plenum during a PCC scenario to monitor the flow phenomena in the upper plenum of the VHTR. INL covered mainly the conceptual design and scaling of possible models. The conceptual design included inducing channel flow with pumps or natural circulation, possible heat sink designs, the fluids to use, and modeling designs that allowed for light sheets to illuminate the upper plenum for particle imaging. The scaling analysis approach was to match the Richardson number, the ratio of the buoyancy force and inertial force, and the Reynolds number, the ratio of inertial to viscous forces, of the experimental model to the VHTR prototype for normal operation of a PCC scenario. The Boussinesq Approximation was used to determine the density change as a function of temperature. The Boussinesq approximates the density change as,

$$\rho = \rho_0 + \Delta\rho \tag{2.1}$$

Using this Navier-Stokes equation becomes [16],

$$\frac{D\overline{V}}{Dt} = -\frac{\nabla P}{\rho} + \nu\nabla^2\overline{V} + \frac{\Delta\rho}{\rho}\overline{g} \tag{2.2}$$

In this $\overline{V}$ is the velocity vector, t is time, P is pressure, ν is kinematic viscosity, and $\overline{g}$ is the gravitational acceleration. Measuring the pressure difference and using it analytically

is problematic. To fix this it can be represented as a function of the temperature difference,

$$\Delta\rho = -\alpha\rho_0\Delta T \tag{2.3}$$

Where α is the thermal expansion coefficient. As discussed before the Richardson number is the focus of the scaling analysis. From the Navier-Stokes equation the inertial and buoyancy forces are used to represent the Richardson as a function of either the density or temperature gradient. The Richardson number and the ratio for the model (m) and the prototype (p) are shown below.

$$Ri = \frac{g(\Delta T / T)D}{V^2} \tag{2.4}$$

$$\frac{\mathrm{R}\,i_m}{\mathrm{R}\,i_p} = \frac{\left(\frac{\Delta\rho}{\rho}\right)_m}{\left(\frac{\Delta\rho}{\rho}\right)_p}\frac{V_p^2}{V_m^2}\frac{D_m}{D_p} \tag{2.5}$$

And if the Richardson number matched for both the model and the prototype, that is $Ri_m / Ri_p = 1$, then the Reynolds number ratio may be expressed as,

$$\frac{\mathrm{Re}_m}{\mathrm{Re}_p} = \frac{V_m D_m \nu_p}{V_p D_p \nu_m} = \left[\frac{\left(\frac{\Delta\rho}{\rho}\right)_m}{\left(\frac{\Delta\rho}{\rho}\right)_p}\right]^{1/2}\left[\frac{D_m}{D_p}\right]^{3/2}\frac{\nu_p}{\nu_m} \tag{2.6}$$

The pressure and temperature difference for the experimental model will be significantly less than that of the prototype as the model can only realistically operate at much lower

temperatures and a pressure near one atmosphere, so the ratios would be off. However if water was used in the experimental model then this problem can be compensated for by the differences in density and viscosity between water and helium. Additionally the experimental model cannot model the Reynolds number in the core. This is due to the decrease in the number of channels from about 11,000 total channels to 67 channels for a $1/4^{th}$ scaled model. Once the flow enters the upper plenum the model may be representative of the Reynolds number. After this other characteristics of the model such as the adiabatic heat transfer and relating the model jet flow and the prototype jet flow were considered for the scaling analysis of the model.

After the scaling analysis was done the INL began the experimental modeling design [17]. Different experimental modeling techniques were considered for modeling a VHTR under normal operations or PCC conditions. The designs covered an experimental apparatus that could model three dimensional laminar natural circulation in the upper and lower plenums. One topic was the method to model the heated coolant. One method was heating the fluid in the core channels to induce natural circulation, another by simulating the channel flows using pumps of pre-heated fluid. For the upper plenum one could use a complete, one-half, or one-quarter model of the geometry of the prototype. The instrumentation was also discussed. The main data acquisition would be performed by PIV and Planar Laser Induced Fluorescence (PLIF) which can measure the temperature field of a planar cross section.

Oregon State University has been tasked with creating a High Temperature Test Facility (HTTF) to model a Very High Temperature Reactor (VHTR) during a DCC

accident scenario [8]. The HTTF will provide benchmark data for existing safety analysis codes. For the modeling it was assumed that the Boussinesq approximation is valid and the fluid is incompressible. This facility would model the DCC conditions where there is a LOCA scenario and air ingress. It is expected that the air being colder would collect in the lower plenum, and transiently diffuse through the helium. As the core of the HTTF will be very hot a ceramic core was designed. The final scaled model was 1:4 length scale and 1:2 time scale. It operates at a temperature of 687 ^{0}C and 259 ^{0}C for the inlet and outlet respectively, but only at a low pressure of 0.8 MPa, so the modeling begins once the depressurization of the prototype is complete[18]. Figure 2-5 shows the geometry of the HTTF [19].

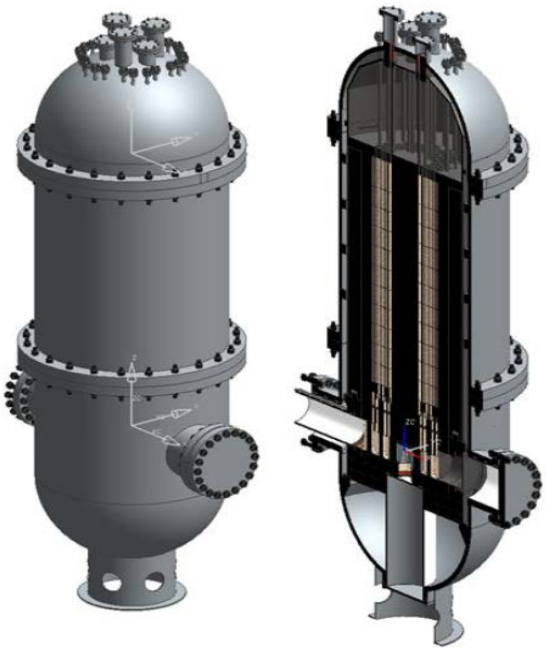

Figure 2-5: Oregon State University's high temperature test facility

2.3 Previous Studies – Particle Image Velocimetry

Particle Image Velocimetry can measure large or small flow fields instantaneously in a non-intrusive manner. This is very beneficial for flow analysis. Figure 2-6 shows a schematic on how PIV functions [20]. PIV is executed by injecting small particles into the working fluid. Two laser pulses are fired in quick succession that illuminates the particles. A high speed camera captures the 2-D laser sheets of illuminated particles. When a picture is taken the high speed camera interprets the intensity of the light reflected by the particles as a value. It takes this value for each pixel and represents this value in a digital image as something similar to a signal.

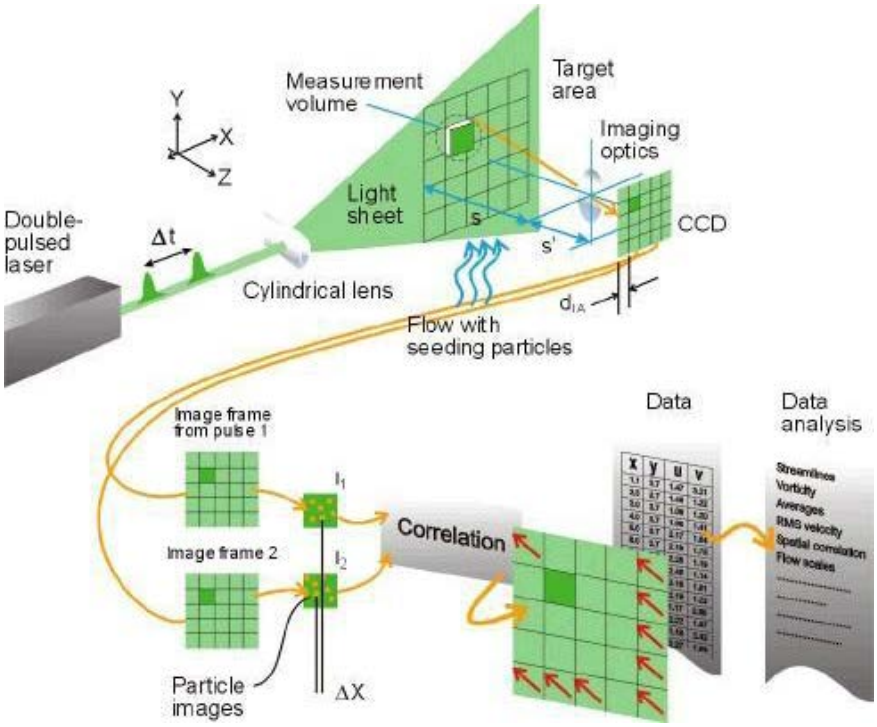

Figure 2-6: PIV schematic

To compare the pictures the images are subdivided into several “interrogation windows”. Each interrogation window is comprised of multiple pixels. Next a cross correlation function is used to compare the two images or image pair. The below equations is used in direct cross correlation.

$$R_{AB}(s) = \iint A(X)B(X+s)d^2X \tag{2.7}$$

A and B store the light intensity of each pixel which can be extracted similar to a matrix. X is the domain of an interrogation window, R_{AB} is a correlation value between an interrogation window of the first image compared with a nearby interrogation window in the second image which essentially represents how close the pattern of one window compares to the other. The variable s is the displacement vector between these two windows.

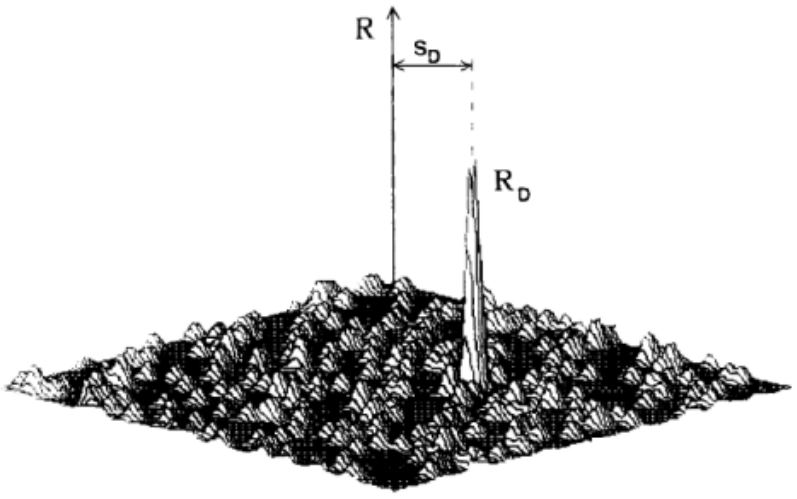

Figure 2-7: Cross correlation field

Cross correlation integrates through the domain of X to give a total correlation value between the two windows. After all nearby windows have been scanned you would have a field of values as represented in Figure 2-7 [21]. S_D would be the displacement vector for that pair of interrogation windows. Once all the nearby windows have been cross correlated then the highest correlation value is selected and the displacement vector is set.

The problem with this method is it is computationally slow. However applying the Fourier Transformation greatly reduces the calculation time, this method is called the Fast Fourier Transformation (FFT), which transforms convolution equations shown in equation 2.8 to equation 2.9 [22]. The cross correlation equation 2.7 has the same form as the convolution equation 2.8 so FFT may be applied to it removing one of the integrals. The cross correlation still needs to scan all the nearby interrogation windows of the paired image, however FFT removes the need to integrate through the domain of X for each window.

$$C_{fg}(\Delta x) = \int_{-\infty}^{+\infty} f^*(x) g(x + \Delta x) dx \tag{2.8}$$

$$C_{fg}(\Delta x) = \mathbb{F}^{-1}[F^*(k) G(k)] \tag{2.9}$$

Using this method one can get the instantaneous velocity field, however sometimes the time-averaged velocity field is of interest particularly if testing for statistically steady state. There are different methods for time averaging[23]. There are

three primary steps in PIV: Obtain the particle images, generate the correlation functions, and then run the peak detection which essentially is generating the velocity vectors. One time-averaging method is the Average Velocity Method, which averages the instantaneous velocity measurements. Instantaneous velocity measurements will have some erroneous velocity vectors, but they can be removed by filters that compare the velocity vectors with nearby vectors and removes them if they vary significantly from the standard deviation of the neighboring images. This study uses this method for the time-averaged velocity field. Another method is to average the images themselves. This can be beneficial when the particle density is low or if the interrogation window is small, although can be detrimental if there is a large number of images. The last method is to average the instantaneous correlation functions for each image pair. This method is good for reducing the noise to signal ratio and also reduces the probablility of erroneous measurements, but must be implemented directly in the PIV code.

When running PIV analysis there can be false or spurious vectors that do not follow the flow regime, by either varying greatly with the neighbor vectors or not being physcially possible. These vectors will occur when either there are an insufficient number of particles or there is a low signal to noise ratio [24]. To correct this an algorithm can be developed to correct the false vectors. The first step in this algorithm is to find a region of coherent vectors. To do this an equation is used to compare one vector with its neighboring vectors,

$$val = \frac{\sum_i |v_i - v_0|}{\sum_i |v_i|} \tag{2.10}$$

Where v_0 is the vector of interest and v_i represents the neighboring vectors. Where this value reaches a minimum represents a region of uniformity. Once found the algorithm sweeps the vector field finding all vectors coherent with the first group by checking the neighboring vectors and seeing if they differ by less than a given amount specified by the user. Once the region has expanded until the neighboring vectors differ too largely the algorithm searches for another region to build off of. The sizes of the region generated will vary in size depending on the uniformity of the flow; in highly turbulent areas the regions may only contain a few vectors. Once all the regions have been generated they are checked again for any deviant vectors. The vectors that do not make it into any regions are removed. This method does require user input values that impact the sensitivity of the algorithm, but experiments have shown the impact to be low.

A study in Japan performed PIV and planar laser induced fluorescence (PLIF) for the mixing process of a turbulent jet[25]. The jet was ejected at a Reynolds number of $2x10^3$ with a jet velocity of 2 m/s. Small particles were injected for PIV and a fluorescent dye was added for PLIF. During the experiment the dye and the particles were recorded separately. The dye was not used to measure temperature but to measure the concentration, 67 frame pairs were averaged at several cross section locations. Using this several profiles of the mean velocity, turbulent intensity, Reynolds shear stress, mean concentration, concentration fluctuation, and the turbulent flux were obtained and validated by comparing the results with previous studies. Due to the short duration of the experiment not enough data was gathered and there was significant discrepancy with

some of the data, particularly with the turbulent flux and concentration fluctuation. To correct this, the study suggested to simply extend the duration of the experiment and to modify the ratio of fluorescent dye and exposure time of the camera.

For normal operation the core operating temperature profile is important, and there may be severe thermal stresses in the lower plenum, but there isn't much of interest in the upper plenum as the coolant is coldest there. For the Depressurized Conduction Cooldown scenario the air ingress occurs in the lower plenum, and slowly diffuses into the core where it oxidizes with the fuel. Multiple computer codes have ran simulations to monitor the phenomena in the core and the lower plenum for both normal operation and a DCC accident scenario, and experimental models have been built to validate the codes. There has been some CFD analysis for the upper plenum for a PCC scenario; however there is no benchmark experimental data to validate the results. The experimental facility that was designed, constructed, and tested in this study can produce results to fill this deficiency of data.

3 PROJECT DESIGN

3.1 Solidworks Design Phase

INL initially provided a rough design shown in Figure 3-1. Initially a $1/8^{th}$ scaled design was considered however the required heat input for modeling a VHTR was too large, so a $1/16^{th}$ scale design was chosen. The basis for the design was a closed loop system where the flow was driven purely by natural circulation. The inlet to the test section would go into the lower plenum where the water is then drawn up through heated pipes by natural convection. The water would then leave the pipes simulating slow jets into the upper plenum, the region of interest. The water would then exit the upper plenum into the downcomer, the region between the modeled core and the outer containment. A heat sink, which they called a water cooling jacket, would need to remove the majority of the heat input so that the system could reach a statistically steady state and to help induce natural circulation. As it goes to the downcomer the water will lead to the outlet and into a reservoir of water from which the inlet pulls water through.

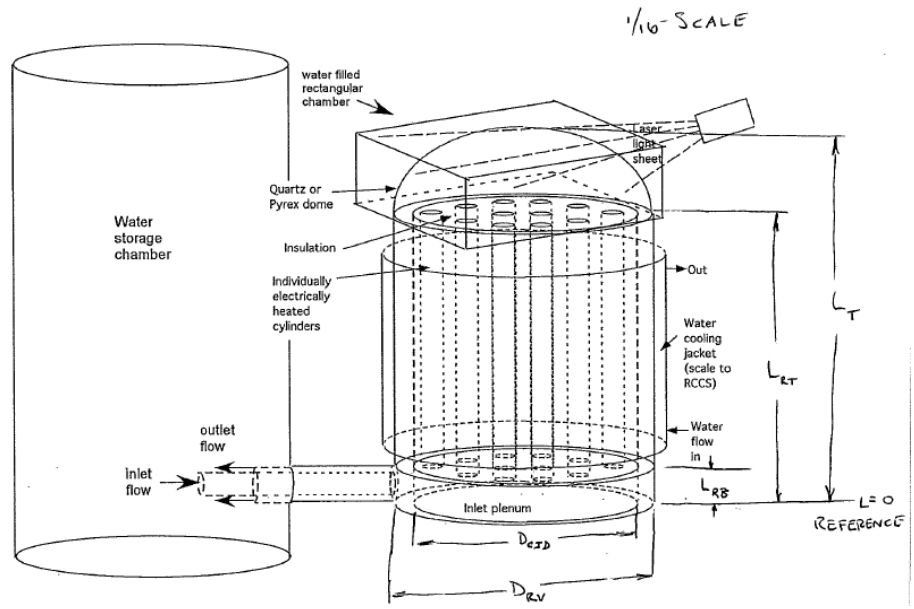

Figure 3-1: Initial design geometry

Initially the design had a concentric pipe that would contain both the outlet and inlet. But during the design phase in Solidworks this was determined to greatly complicate the model and would make the assembly and fabrication challenging. Two separate pipes for the inlet and outlet were used since the region of interest was the upper plenum and having the inlet and outlet be two separate pipes wouldn't affect the experimental testing or results. Next the pipe layout needed to be determined. Through collaboration INL made the final design of 25 pipes with a ¾ inch inner diameter arranged in a hexagonal pattern equidistant from each other, as shown in Figure 3-2. Initially an annular pattern was considered however the pipes needed to be equidistant and that wasn't possible for the annular design, so a hexagonal pattern was used instead.

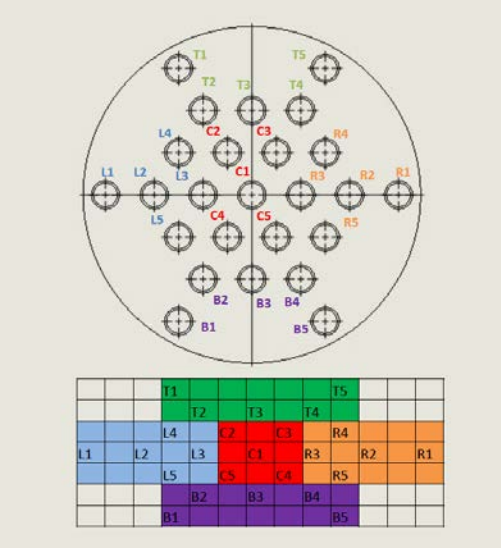

Figure 3-2: Pipe layout

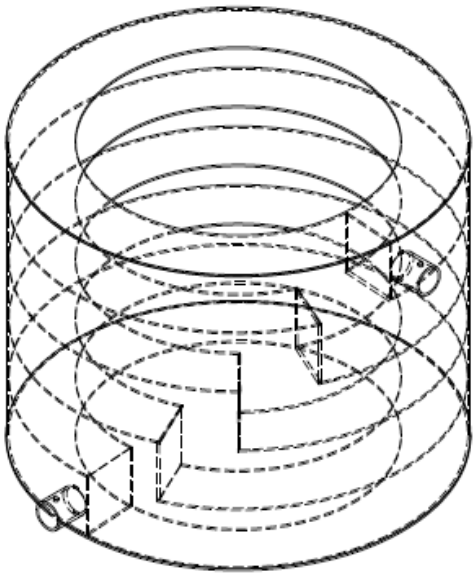

Figure 3-3: Cooling jacket design

For the heat sink multiple methods were considered. Typically to remove heat from fluid a series of coiled tubing is built into the flow path and cold water is pumped through them. For our design the tubing would go between the outer containment and the

core containment. However that would create a large pressure drop for our system which is already at a low pressure differential since there is no pump being used. This means that the heat removal must be external. To design an external uniform heat removal cooling jacket a series of baffles that would be connected to the outside of the containment. This means the material needed a high thermal conductivity, stainless steel was chosen. The final design included a series of five baffles where the water would be pumped into the bottom, circulate around the containment, and then rise 3.5 inches and repeat the process until it reached the outlet of the cooling jacket, shown in Figure 3-3.

Next the design process for all the parts began. The geometry from INL included only the measurements for the fluid region. Free reign was given for designing the experimental components. When designing the largest parameters were how to have waterproof access to the core for wiring, fabrication limitations, ease of assembly and disassembly, and data acquisition. Four iterations of designs were considered and discussed with the fabricators and colleagues, mainly deciding how to waterproof and have access for wiring, until the final design was chosen and shown in Figure 3-4 and Figure 3-5.

All grey parts are made of polycarbonate and the blue parts are stainless steel. Polycarbonate was chosen for its opaqueness and the ability to withstand high temperatures, as well as ease to manufacture. Stainless steel was chosen for its conductivity, durability, and price. The lower plenum was straightforward, the inner diameter and height were determined by the reference geometry. On top of the lower

plenum sits the core containment which is connected by a flange and sealed with an O-ring. The core containment starts with a two inch plate. In the center of the plate there are 25 x 3/4 inch holes that match the ID of the piping chosen. At the edge of the plate 10 holes located radially are drilled in from the edge, and then holes are drilled on the top of the plate that intersects with the other holes. This is used for wire access to the core. A one inch high cylinder is cut into the center of the plate which will be discussed later. Next a large hollow cylinder was welded onto the plate which acts as the core containment.

Next is the outer containment to which the cooling jacket is welded. It sits on the core containment and is sealed with an O-ring. A 3/4 inch gap exists between the core containment and the outer containment as given by the INL geometry, this acts as the downcomer for the fluid. A large diameter outlet was chosen so the fluid may enter it easily. The cooling jacket was not placed at the exact exit top of the containment

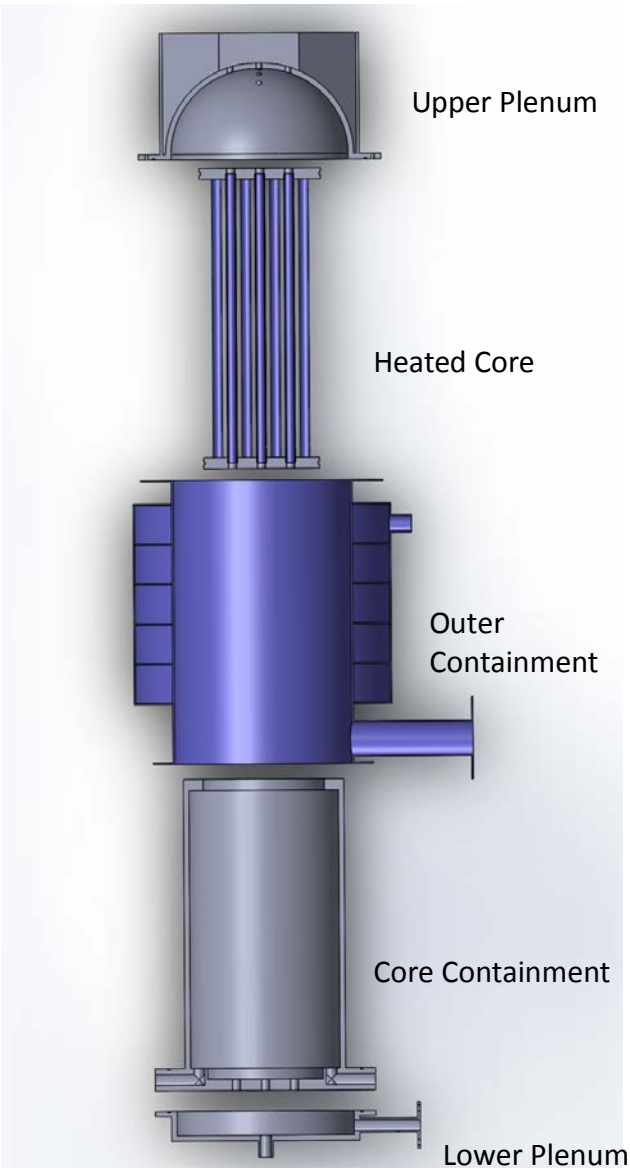

Figure 3-4: Exploded cross section

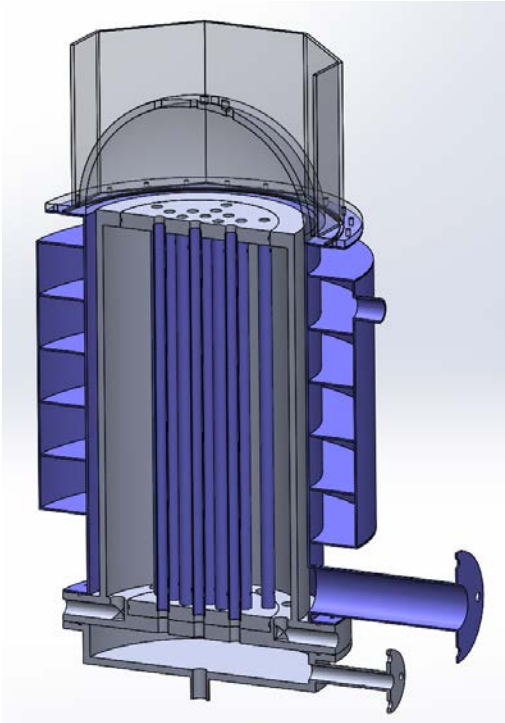

Figure 3-5: Cross section after assembly

because the last baffle wouldn't be perfectly uniform since the temperature of the fluid will rise as it circulates the downcomer, lowering it a few inches would inhibit the affect it will have. Next the core can be inserted. The core consists of a bottom plate with a 10.5" diameter and 1" thickness. It has 25x 3/4" holes that are countersunk 1/2" to match the outer diameter of the steel pipes. The twenty five steel pipes are inserted into these holes each of which has their own O-ring. The steel pipes have two threaded holes near the top and bottom of the pipe that can be used for compression fittings for thermocouple

access. The top of the pipes are then inserted into the top plate which is similar to the bottom plate but has a diameter of 11". Once the core is assembled it may be dropped into the core containment. The top and bottom plates seal the containment with O-rings.

Finally the upper plenum is placed on top of the steel containment where it is sealed with a flange and O-ring. Again the half-sphere geometry was designed to match INL's specification. The top of the sphere has nine threaded holes for compression fittings for thermocouple access to the upper plenum. A correction box is glued outside the dome which is used to correct the distortion from looking onto a curved surface filled with water. Once the correction box is filled with water a flat surface is presented that can be used for imaging. Originally a square box was used but this limited pictures to be taken on four planes and had bolts for the flange inside the correction box which would be difficult for assembly. Instead an Octagonal shape was chosen. With this the final design was sent to the fabricators.

3.2 Project Assembly

As the parts were being fabricated the thermocouples were made to measure the temperature rise in the piping, cooling jacket, and inlet and outlet of the system. After consulting with Omega, a thin T-type thermocouple was selected. The wire was cut into approximately seven foot lengths. One end was stripped and welded together with an arc welder. The thermocouples were hooked up to a National Instruments data acquisition system and measured with Labview. They were then calibrated with a Fluke Thermometer at the approximate temperatures of 20 ^{0}C and 80 ^{0}C. Once this was

completed the steel piping with the threaded holes were acquired early since their machining process was simple and short. Compression fittings were screwed into the pipes and thermocouples were installed. To test for leaks one end of the pipe was sealed while the other end had an extended pipe attached to it to simulate the head pressure it would be operating under. Originally Teflon tape was used to seal the thread, however only nine out of ten were successfully sealed. Different techniques were considered such as using epoxy but eventually it was decided to take them to a welding shop and weld the compression fittings to the pipes to fully ensure they wouldn't leak. After this the scaffolding to house the experiment was designed and constructed. Unistrut beams were used to construct it, the design is shown in Figure 3-6. Many supports were built under the experimental facility and the water reservoir.

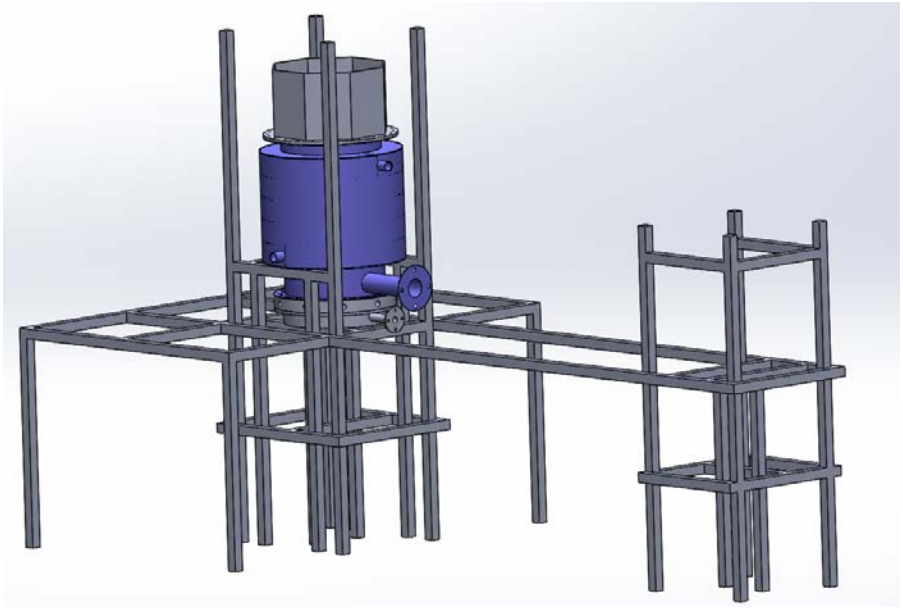

Figure 3-6: Experimental scaffolding

Next the twenty five heating tapes were acquired and tested. The average resistance was approximately 89 ohms with a standard deviation of 2. The heating tapes would be controlled by five variable voltage transformers. The piping was broken into five groups of five as shown in Figure 3-2. The heating tapes were grouped by similar resistances. When we finished testing the heating tapes the machining of the experiment's parts completed. Figure 3-7 shows the pipes with heating tapes and thermocouples inserted into the bottom plate. Figure 3-8 shows the core containment on top of the lower plenum. The design allows the core pipe configuration to be oriented with the inlet in different patterns. One could either have three pipes in line with the inlet and seven pipes in the symmetric plane, or vice versa. This assembly had the core containment bolted onto the lower plenum such that the seven pipes would be in the symmetric plane. Figure 3-9 shows the reservoir tank which was selected so the height would be greater than the experimental facility's height.

Figure 3-7: Piping, heating tape, and thermocouples

Figure 3-8: Lower plenum and core containment

Figure 3-9: Reservoir tank

Next the insulation for the core was installed. The insulation was important to keep any heat from leaving the core and heating the downcomer which would inhibit the natural circulation. A high temperature ceramic insulation that uses aluminum silica was selected. It was cut into strips and inserted between the pipes. Then a larger sheet was wrapped around the core and taped as shown in Figure 3-10. Ropes were looped down one pipe and up a different pipe to lift the core and drop it into the containment wherein the ropes would be extracted. The core was slowly lowered into the containment and the wires were drawn out through the holes. Once installed more insulation was stuffed around the outside shown in Figure 3-11.

Figure 3-10: Insulated core

Figure 3-11: Core and containment

Once installed the top plate of the core needed to be sealed. With a coordinated effort the twenty five pipes were line up with the plate and force was applied till the O-rings were sealed and the plate was flush shown in Figure 3-12. Next a lift was used to lower the steel containment around the core containment shown in Figure 3-13. Once the

lower flange was sealed the upper plenum was placed onto the steel containment and bolted in. A custom gasket was made to seal the upper plenum and steel containment since the flange on the steel containment was wavy and not level.

Figure 3-12: Top plate flush with containment

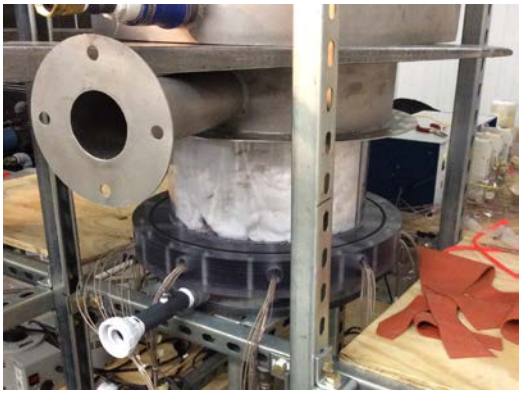

Figure 3-13: Outer containment being lowered

Now the test facility was ready to be attached to the reservoir and filled with water. Figure 3-14 shows the view of the assembled facility filled with water and Figure 3-15 shows the top view of the upper plenum to show the inlet pipes and the

downcomer. It should be noted that there was one difference between the design and machined parts. When forming the dome of the upper plenum a sheet of polycarbonate is heated till its malleable and then sucked into a vacuum creating a bubble. The height of the dome is determined by how much the plastic could deform before it hardened. The dome size made by the fabricators was insufficient to match the height of the design. To compensate for the difference in height between the design and the fabricated dome the remaining height was glued on as a cylinder. This was deemed insignificant in altering the fluid behavior for generating benchmark data. Once the facility was attached to the reservoir and filled there were some external leaks in the piping but they were fixed by adding additional Teflon tape and gaskets where needed. Once the leaks were fixed a few tests were run to perform the shakedown of the test facility. A shakedown is essentially a process where the facility is tested to confirm everything is working in proper order. A few thermocouples had broken in the installation process. Most could be

Figure 3-14: Assembled facility

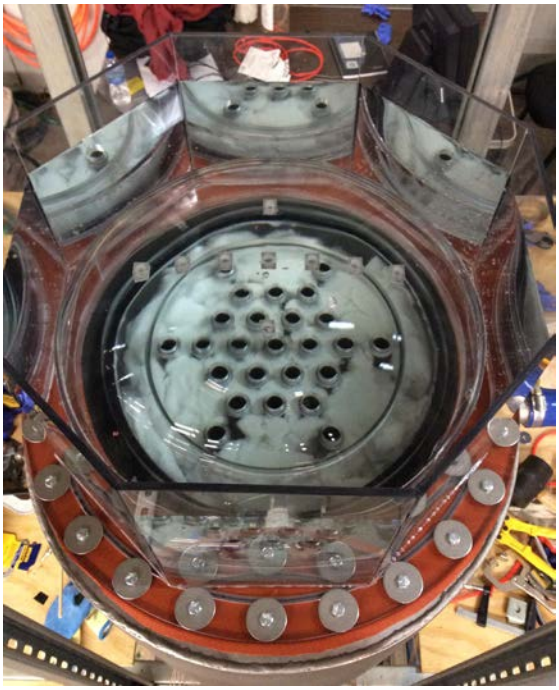

Figure 3-15: Top view of upper plenum

fixed externally by splicing the break in the wire, but two remained broken inside the core and inaccessible. After the facility was filled about five times we noticed something was wrong with the heating tapes. When five heating tapes are grouped in parallel the total resistance is approximately 18 ohm. However two of the groups read around 22 ohms indicating that two heating tapes had failed. Moisture had slowly leaked into the core, soaked into the insulation, and gotten some heating tapes wet. This caused the heating tapes to fail. Unable to operate with a non-uniform core and the risk of shorting more heating tapes meant the facility had to be disassembled and the leak addressed.

The source of the leak could not be determined from the disassembly, but it was likely from the bottom of the core as the insulation was moister and was at a higher pressure. There were several possible causes though. One was the thermocouples connected to the compression fittings. They were originally sealed into the fittings using Teflon tape and they passed the test but over time a few of them may have begun leaking. Another possibility was the pipes connection to the bottom plate using the O-rings. No lubricant was used when inserting the pipes into the O-rings so some of them got damaged in the assembly. The last possibility was the groove on the bottom plate for the large O-ring was close to the countersunk holes for the pipes furthest from the center. To account for this possibility a thin layer of epoxy was applied at possible leak locations. For the O-ring problem the damaged O-rings were replaced, and a lubricant could be used in the next assembly. To prevent the leaking from the compression fitting would require extra work.

First no matter what precautions were taken there would still be the possibility something would fail. To protect the heating tapes each heater was water sealed individually. To accomplish this first heat shrink tubing was used to seal the leads coming from the heaters. Next high temperature silicon tubing was wrapped around the heaters and sealed with a high temperature adhesive. The pipe was clamped until the adhesive was dry as shown in Figure 3-16. This tubing sealed the pipes from water and also acted as insulation. Once this was completed for all 25 pipes a partial reassembly was done. It was the same as the previous assembly except lubricant was used and the assembly stopped before the core was sealed off. The facility was filled up to the top of the pipes. This confirmed that there was some leakage from the thermocouples. Thermocouples are two wires with a plastic coating holding them together. Between the wires there is a groove that may have been the cause of the leak. The next step was to seal off the thermocouples.

Figure 3-16: Sealing the heating tapes with silicon tubing and adhesive

Once all the broken thermocouples were replaced a new method of inserting the thermocouples into the compression fitting was devised to prevent leaks. Fine steel tubing was cut into short lengths and the thermocouples were threaded through them. The thermocouple was then sealed on both ends of the tubing with a UV epoxy. UV epoxy is liquid until a UV light is shone on it which causes it to harden in a few seconds. After this ferrules are slid over the tubing. When the compression fitting is tightened the ferrule clamps down on the tubing causing it to compress and seal. The final result is shown in Figure 3-17.

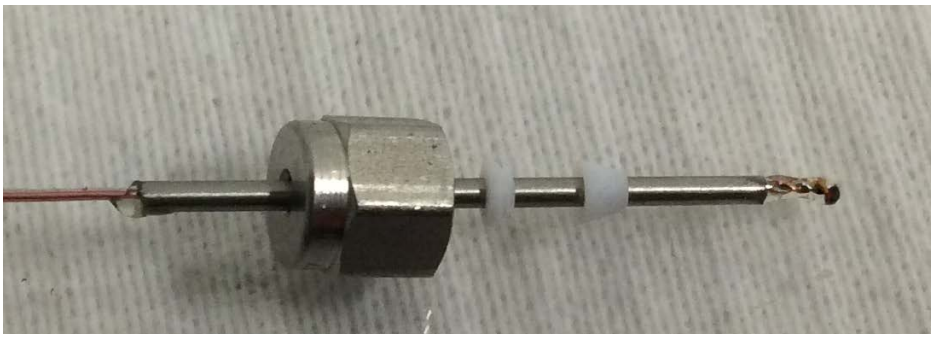

Figure 3-17: Thermocouple with tubing, epoxy, and ferrules

Once completed for all 50 thermocouples a few more tests needed to be performed before reassembly. The heating tapes and thermocouples were tested and all functioned properly. A partial reassembly was performed and tested for leaks and none shown. Satisfied a ring of insulation was added around the core, and the top plate was inserted sealing off the core shown in Figure 3-18. This was much more difficult as the silicon tubing had to be compressed slightly to allow all 25 pipes to simultaneously line

up with their holes, but was accomplished using clamps. Once completed the upper plenum was installed and the reassembly finished, the facility was ready to start testing.

Figure 3-18: Core top view after reassembly

3.3 Data Acquisition

The experimental facility has several data acquisition devices installed to monitor the test that can be used to produce benchmark data for CFD validation. This is outlined in Figure 3-19. The first measurement is the thermocouple to read the temperature at the inlet to the facility. Then as the water flows up through the core thermocouples measure the temperature rise in all 25 pipes. When the fluid enters the upper plenum PIV is performed to record the velocity flow field. The fluid then goes to the downcomer and to the outlet. A pressure transducer will measure the pressure difference between the inlet and the outlet. On the outlet pipe an ultrasonic flowmeter will measure the total flow rate of the system.

Since the thermocouples were made and not purchased there is no accuracy range. To calculate the precision of the thermocouples the standard deviation may be

calculated post-test. The accuracy can be calculated by inserting a trusted reference thermocouple into the upper plenum and measure the temperature at the outlet of the pipes during the test, and comparing that measurement with the thermocouples that were made. For all data recording a SCXI -1600 model DAQ with three control modules was used. The differential pressure transducer is from Honeywell and could measure a range of +/- 0.5 PSID with an accuracy of +/- .25% of the full scale. The cooling jacket used a paddlewheel flowmeter that had a range of 3-30 GPM and an error of +/- .06 GPM. The flowmeter for the coolant loop of the system was an ultrasonic flowmeter from Krohne. An ultrasonic flowmeter was used because it is non-intrusive. It was attached to the 3" outlet pipe to obtain a better signal and higher accuracy. The flowmeter had an error of +/- 1% if the flow was greater than 0.5 m/s. However since the natural circulation flow was much less than that it was calibrated with a Optiflux 1000 Electromagnetic flowmeter that had an accuracy of 3% at the slow flow rate the experiment was running at.

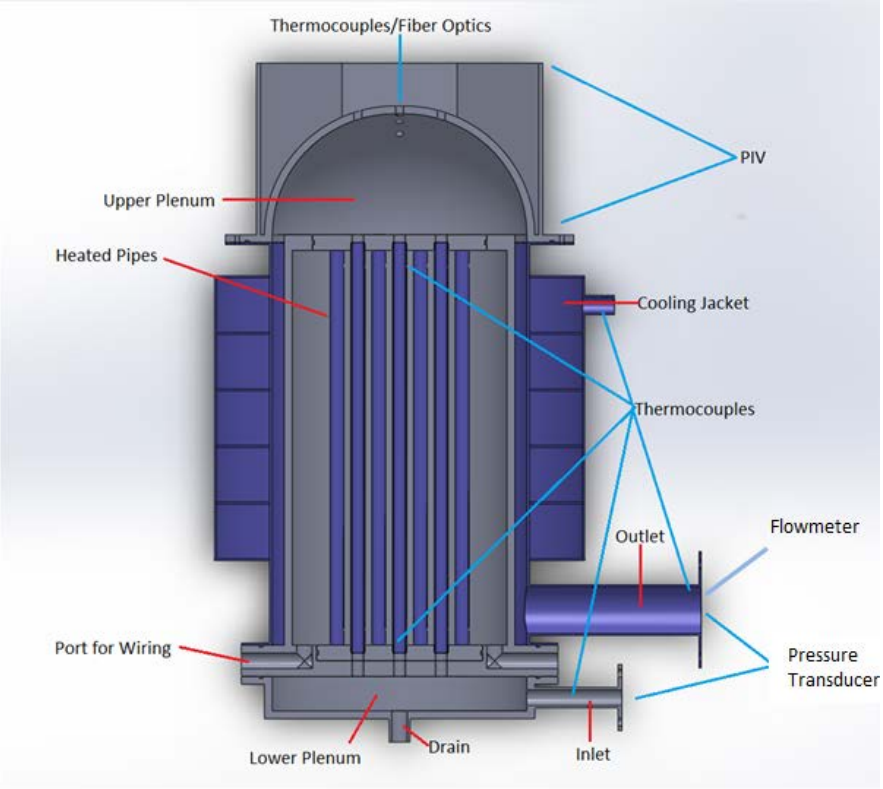

Figure 3-19: Cross section for data acquisition

A separate pipe was connected in line with the Optiflux flowmeter as shown in Figure 3-20. The ultrasonic flowmeter measured significantly but consistently different from the electromagnetic flowmter. The ultrasonic flowmeter recorded the flow for seven minutes and the averaged flow rate was compared to the flow rate measured by the electromagnetic flowmeter. This was performed at six different flow rates between 0.2 and 1 GPM. Shown in Figure 3-21 the data fit a linear trendline well, and the equation was used to correct the flow rate measured in the tests.

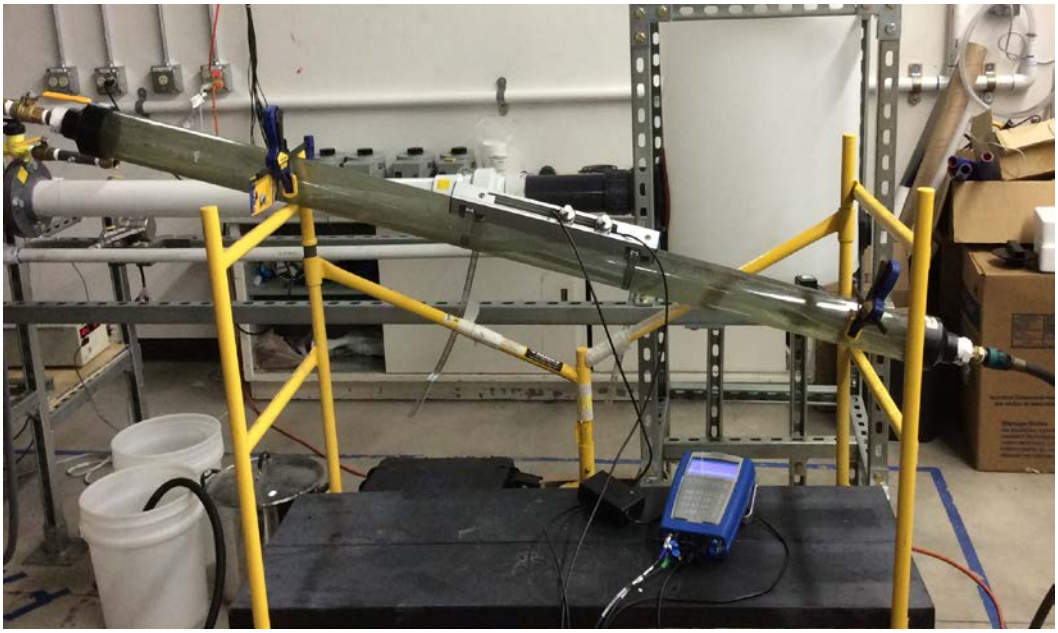

Figure 3-20: Calibration test for flowmeter

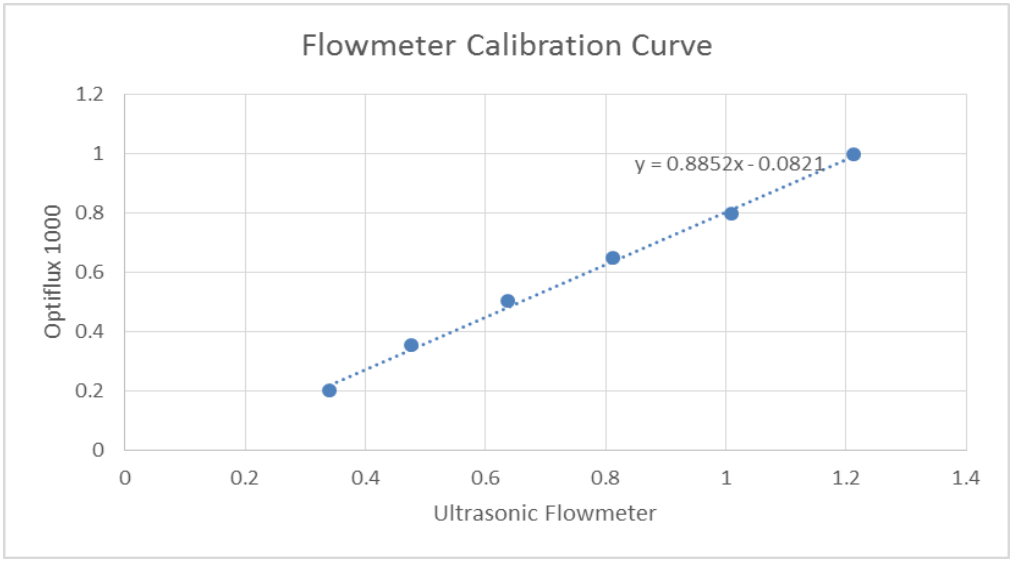

Figure 3-21: Calibration curve for flowmeter

For the PIV system a Vlite series dual pulse laser system that operated at a wavelength of 532 nm and had a frequency range of 1-15 Hz was used. A High speed

camera MEMRECAM GX-3 was used for the imaging. It produced high definition images with 1280x1024 pixel size. The camera and laser were connected to a waveform generator that timed the pulse and the shutter of the camera to activate simultaneously. Next the correct particles needed to be chosen. Initially 20 micron glass bead particles were used. However the pictures taken had light ”noise” from the laser reflecting off parts of the experiment and illuminating small scratches on the plastic which would block vision of the particles. The final particles used were fluorescent polyethylene microspheres which ranged from 20-40 microns. The densities of these microspheres were 1.002 g/cc so the difference in density with the fluid would have a negligible effect on the particles tracking the fluid. The fluorescent particles would reflect the light from the laser as a different color so a filter could be used on the camera that would remove the 532 nm wavelength green color of the laser. This resulted in a much clearer image, as shown in Figure 3-22.

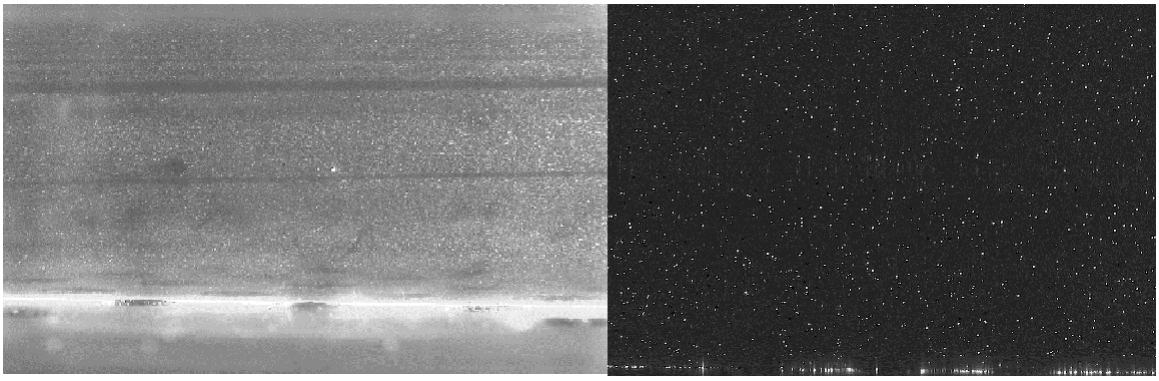

Figure 3-22: Glass bead particles vs Fluorescent particles

4 TESTS AND RESULTS

4.1 Testing

When booting up a test water is pumped into the reservoir which simultaneously fills the experiment equaling a total of approximately 50 gallons. Once filled and no leaks were detected the heaters were turned on. The heating tapes are essentially electric coils around the pipes. When 25 of the electric coils are turned on an electromagnetic field is generated. This put a small voltage in the water. The thermocouples uses a voltage signal so whenever the heaters are on the thermocouple values are greatly skewed, however as soon as the heaters are off they function normally. This means that measurements can't be made continuously for transient measurements, but the heaters could be turned off, data recorded, and turned on again for steady state measurements. Additionally touching the cooling jacket and another metal object would induce a small shock.

For this study only one group of five pipes were turned on and the outlet of three of the pipes were studied, as shown in Figure 4-1 and Figure 4-2. Initially the testing was focused on generating quality images that could be processed with PIV software. Several parameters were tested until an optimal setting was chosen. The laser power level was adjusted till the optimal power output was found. Too much and there would be noise and the particles could not be detected, too little power and the particles wouldn't reflect enough light to be detected. Next the camera was tested. A mount for the camera was constructed that allowed it to move in three dimensions until the desired window was chosen. Eventually the camera was mounted approximately 90 cm away from the

correction box and a magnification lens was used to record the region shown in Figure 4-2. The cross section includes three adjacent jets. Because PIV gives 2-D components for the velocity vectors the other two pipes should have an insignificant effect on the velocity profile. If stereoscopic PIV was used that returned 3-D components then the flow profile may be altered.

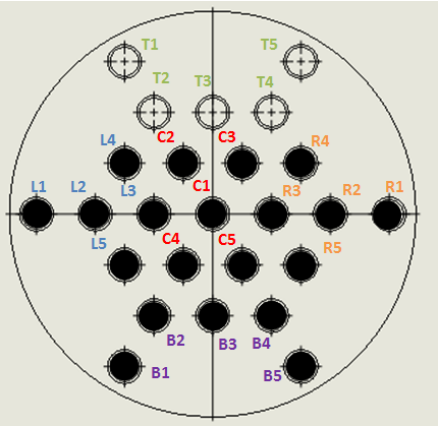

Figure 4-1: Pipe layout with closed pipes

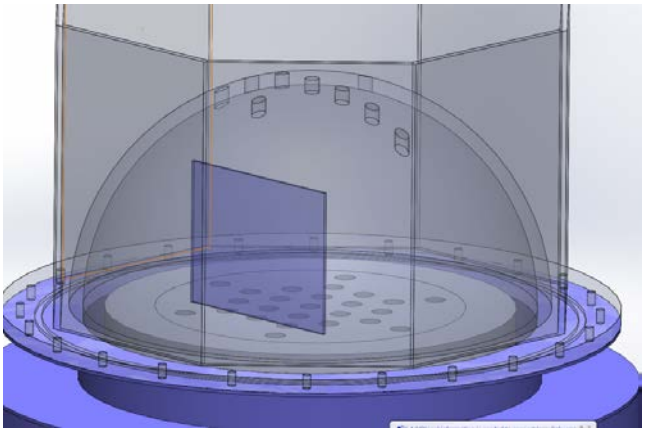

Figure 4-2: Analysis region

Once the camera and laser were mounted appropriately the test was prepared for steady state data recording. Previous testing revealed that stead state was when the outlet of the pipes into the upper plenum reached 45 ^{0}C, this is when the cooling jacket was turned on. The maximum flow rate for the cooling jacket was approximately 10.7 GPM determined by the head pressure at the research building. The flow could be controlled by opening and closing a valve, but the tests were run with the full flow rate. To monitor reaching steady state the outlet of the core piping was monitored, as well as the inlet and outlet of the apparatus. The cooling jacket removed a sufficient amount of heat such that

the inlet and outlet temperatures were less than 1 ^{0}C different. It took approximately 90 minutes to reach steady state.

Once steady state was achieved particles were injected into the inlet of the experimental apparatus. This was allowed sufficient time to circulate into the upper plenum before data was recorded. Then the camera began logging pictures at a rate of 10 Hz, and the flowmeter began logging data. The camera memory can hold approximately 2200 images so the memory is full after four minutes of logging data. Once full the laser was turned off, the flowmeter stopped logging data, and the heaters were turned off so that Labview could record the temperature and pressure differential. This was run five times with the camera in the same position, however two of the times the flowmeter didn't save the data so three sets of data were analyzed for this study.

4.2 Analyzing

Now that the images were acquired the PIV software needed to be selected. After trying different open-source programs PIVlab was selected. PIVlab was written with a Matlab script. It has good processing speeds, data output format, image pre-processing, vector validation, and can make videos of the vector fields. It is also easy to use with minimal experience. Using PIVlab the 2000 images were imported into PIVlab with a 1-2, 3-4 format giving 1000 image pairs as it was estimated that 1000 image pairs would be more than enough to record statistically steady state. Before running the image pre-processing may be modified, such as the interrogation window size. For this test ran two passes with 64 and 32 pixel sizes. When ready all thousand images are processed and a vector is generated for each image pair. Next is the vector validation. PIVlab runs

through all the images with an algorithm as described in the literature review. This removes the false vectors, which would result with NaN values in the output files. Instead the removed vectors are replaced with interpolated vectors. Figure 4-3 shows a vector field of one image pair after vector validation. The orange vectors are the ones that were replaced.

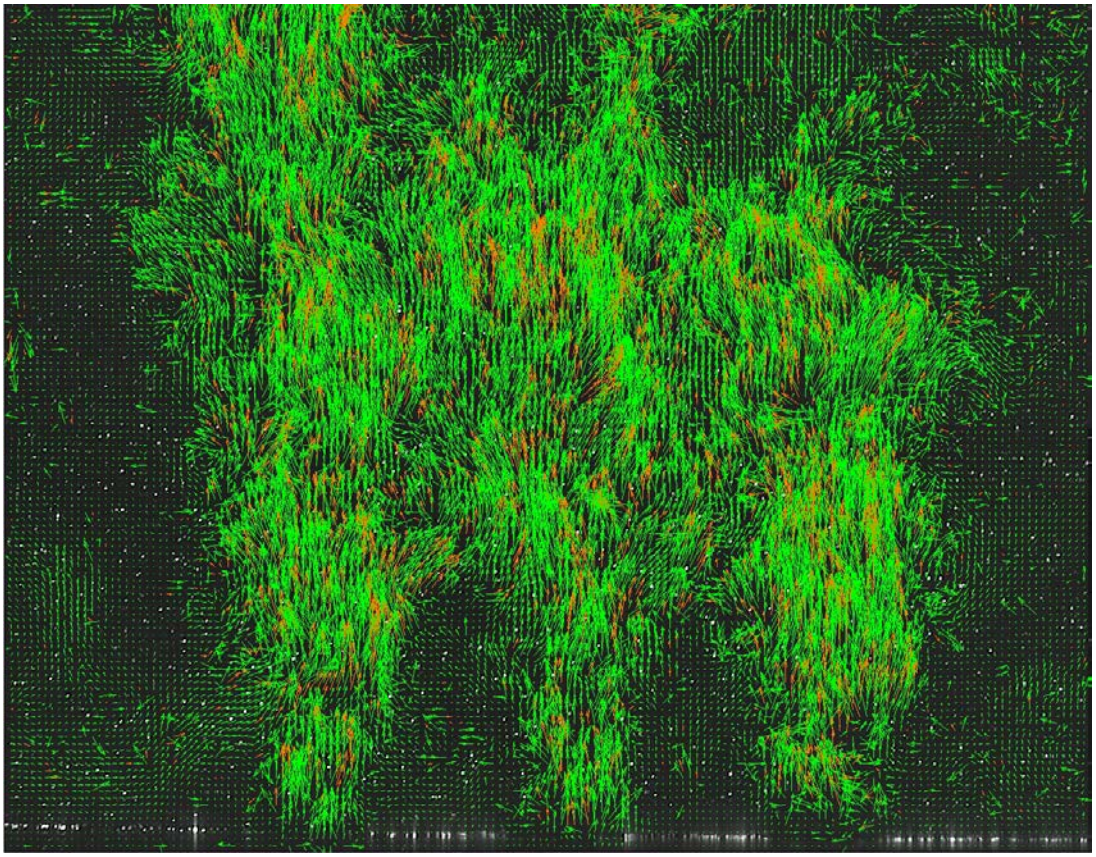

Figure 4-3: PIVlab vector field output

Once all the image pairs are fully processed the flow fields can be saved as a movie, image sequence, or saved as separate text files. The text file data is saved in five columns: x coordinate, y coordinate, x-velocity u, y-velocity v, and vorticity w. This

study is interested in analyzing the statistically steady state. To do this the data must be averaged over a set of image pairs. A sensitivity analysis must be performed to determine how many image pairs are necessary to appropriately model the statistically steady state.

4.3 Results

First a Matlab program was developed to average the velocity vectors generated by PIVlab. This was performed for varying numbers of velocity fields from 20 up to 1000. The 1000 averaged velocity vector field was uploaded into Tecplot where the velocity magnitude was calculated. Next a 100x100 grid is created and the data is interpolated for each grid point. The velocity magnitude is plotted in Figure 4-4. Because PIVlab was written in a Matlab code it sets y=0 at the first row of the matrix and y increases with each successive row.

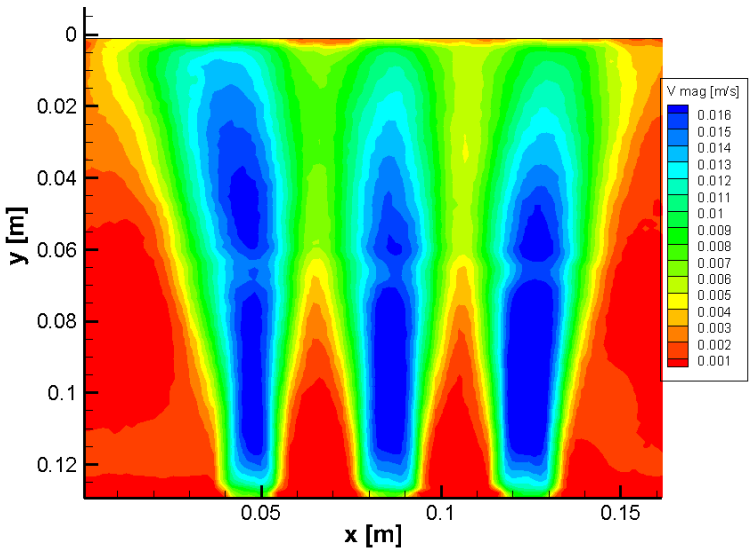

Figure 4-4: Velocity magnitude for set 2

From this contour a few distortions are apparent. First is the distortion at y=0.06 m. This is due to the glued section between the curved part of the dome and the cylinder in the upper plenum which blocks the laser sheet. This casts a shadow where particles would not be illuminated. If the particle can move past the shadow it may still be tracked. This isn't a large issue, when extracting data for benchmarking data at the distortion will be avoided. Another irregularity is the maximum velocity should be at the outlet of the pipes, this is because the images included part of the polycarbonate plate at the bottom of the pictures that were used for PIV analysis.

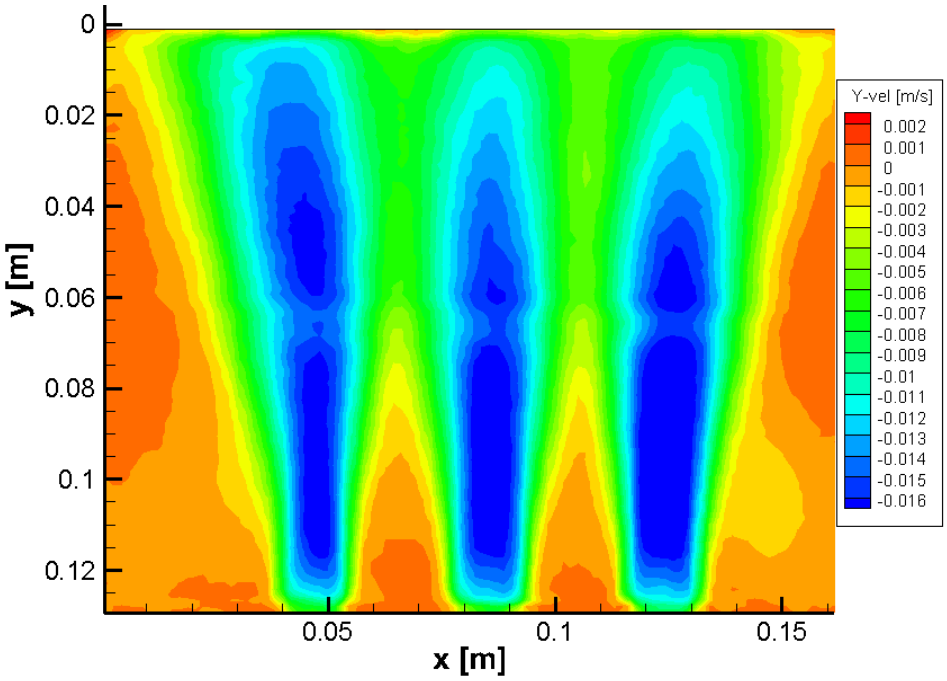

Figure 4-5: Y-velocity contour for set 2

With insufficient particles leaving the pipes PIVlab occasionally may not have a sufficient particle density to run the PIV. This would result in assigning a zero vector

there. If this happens regularly then when the averaged velocity vectors over multiple image pairs the representative velocity would be lower than that of the actual velocity. There are multiple possible methods to correct this. One is to increase the number of particles that are seeded, although this would likely only reduce the error, and the value would still be misrepresentative. Another option is to use a PIV code that recognizes when there are no particles to track and either interpolate it from neighboring interrogation windows, or apply a NaN value. Lastly and likely the surest method would be to use Particle Tracking Velocimetry (PTV) which follows the individual particles and does not use interrogation windows. Similar to the last misrepresentation, data can be extracted elsewhere that PIV functioned properly. Almost all of the flow is in the y-direction, the Y-velocity contour in Figure 4-5 nearly matches the velocity magnitude contour.

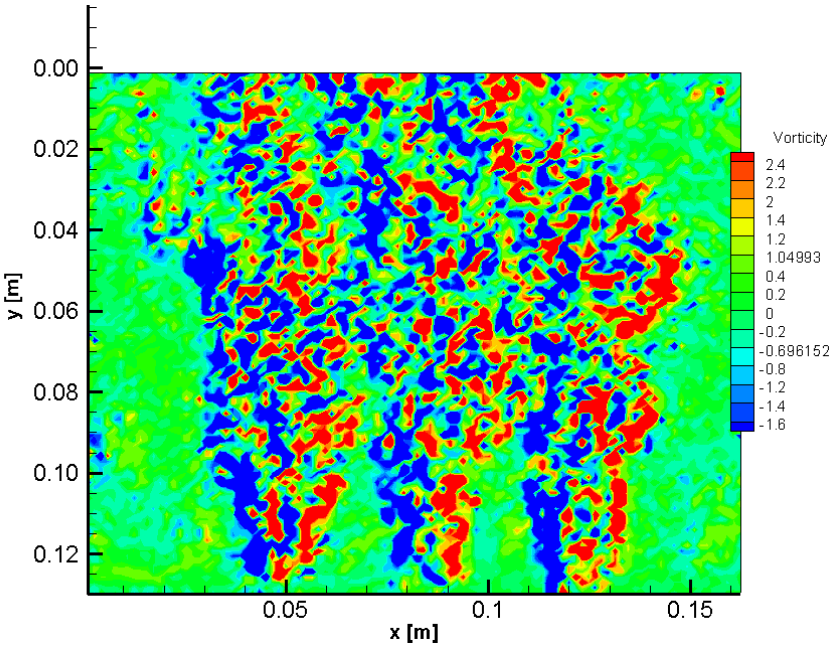

Figure 4-6: Vorticity for single image pair

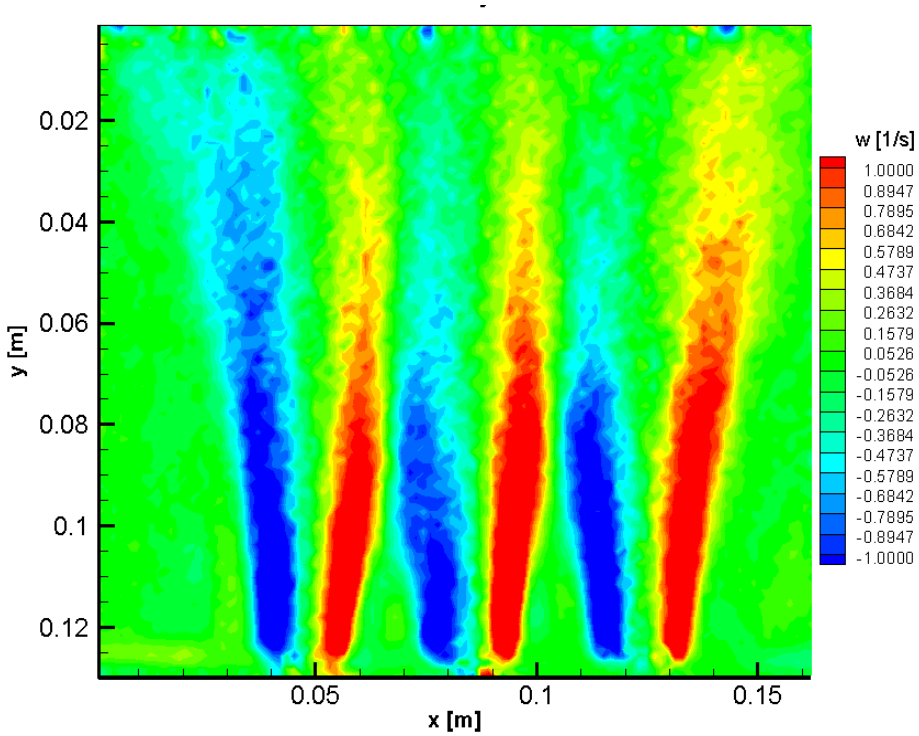

Figure 4-7: Vorticity contour for set 3

Figure 4-6 shows the vorticity field for a single image pair. The negative values represent counter-clockwise rotation or eddies, and the possitive would be clockwise eddies. There is some disorder but a trend can be seen. Once averaged over 1000 image pairs shown in Figure 4-7. This shows the expected antisymmetric behavior expected from jets. Next a scaling analysis was performed to determine the required number of frames to correctly model steady state. The root-mean-squared (RMS) deviation was applied for varying numbers of frames.

$$Error = \sqrt{\frac{\sum_{i,j=1}^{n}\left(\frac{v_{i,j} - \overline{v_{i,j}}}{v_{\max}}\right)^2}{N}} \tag{4.1}$$

In this equation $v_{i,j}$ represents the Y-velocity field for each frame, $\overline{v_{i,j}}$ represents the averaged Y-velocity field for 1000 frames, $v_{\max}$ is the maximum velocity along the jet, and N is the number of frames or image pairs. The percent error is graphed in Figure 4-8. Set 1 differs greatly from sets 2 and 3 which behave as expectedly with the error decreasing exponentially. After reviewing the images from the tests set 1 has less particle density than the other tests, which is likely the cause of the difference and suggests it may not be representative of the flow. More tests would need to be done to confirm this. However they both show approximately a 5% difference between a 700 frame and 1000 frame average.

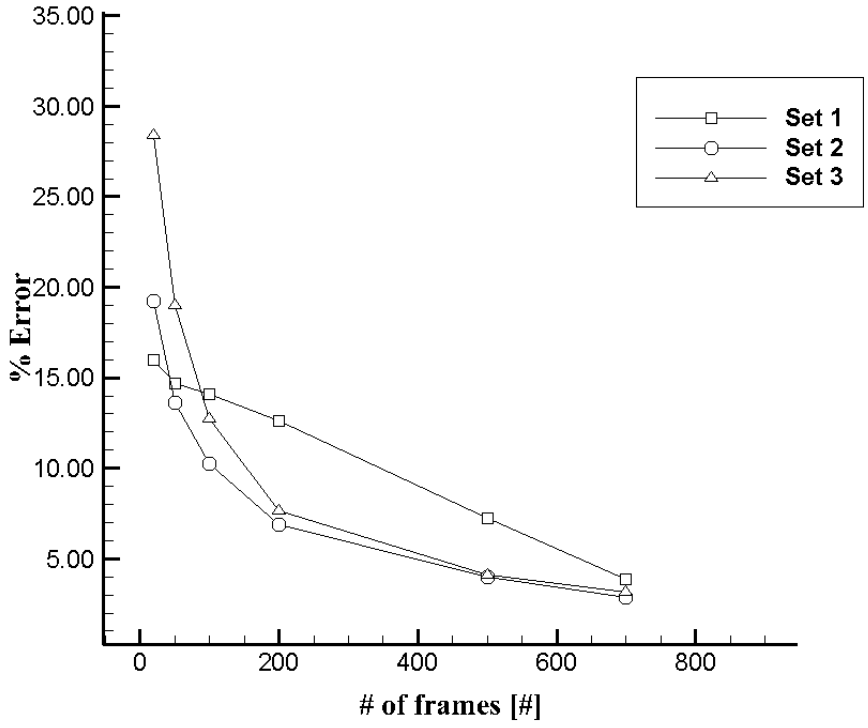

Figure 4-8: Percent error of Y- velocity field for different numbers of image pairs

To further analyze the descrepancies between the sets, lines of data were extracted at different destances from the outlet depicted in Figure 4-9. The sensitivity analysis at the closest slice in Figure 4-10 shows near the outlet pipe a smaller batch of frames can still be representative of the flow.

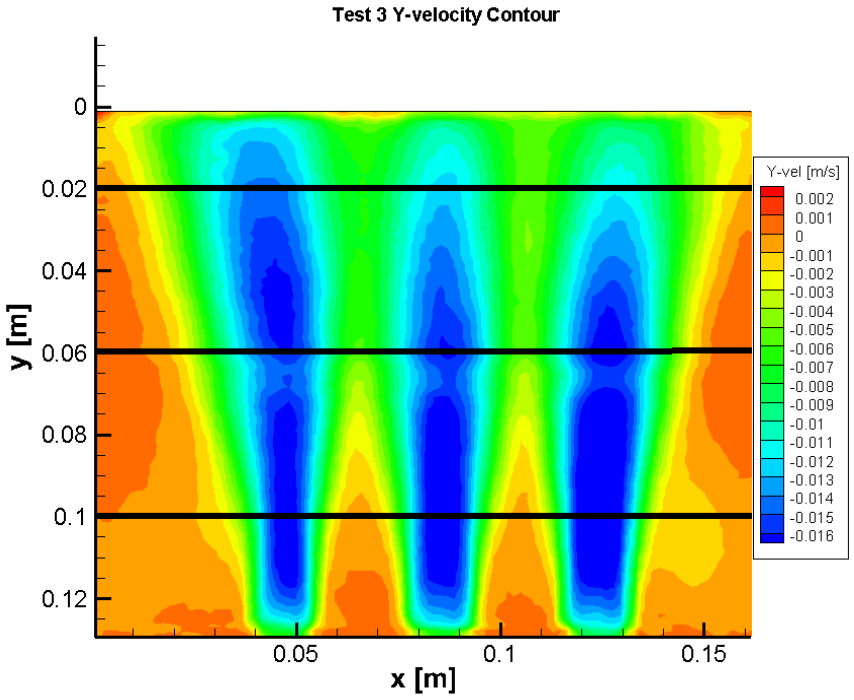

Figure 4-9: Line extraction locations for sensitivity analysis

As the flow goes further from the pipe there is a more significant difference between the frame counts. The extracted data from Figure 4-11 shows that 500 and 700 frames still follow the curve closely and would be sufficint to represent the steady state flow. However the data in Figure 4-12 shows that at about 11 centimeters from the outlet there is a significant difference between 700 and 1000 frames. This suggests that 1000

frames may not be sufficient to correctly model the fluid flow when benchmarking data far from the outlet, and would have to be tested by using more frames. Additionally the peaks and valleys begin to merge suggesting they will eventually become indiscernible and the flow would consist purely of turbulent eddies. The sensitivity analysis was performed for the other sets and shows similar behavior as set 2, the figures may be found in the appendix.

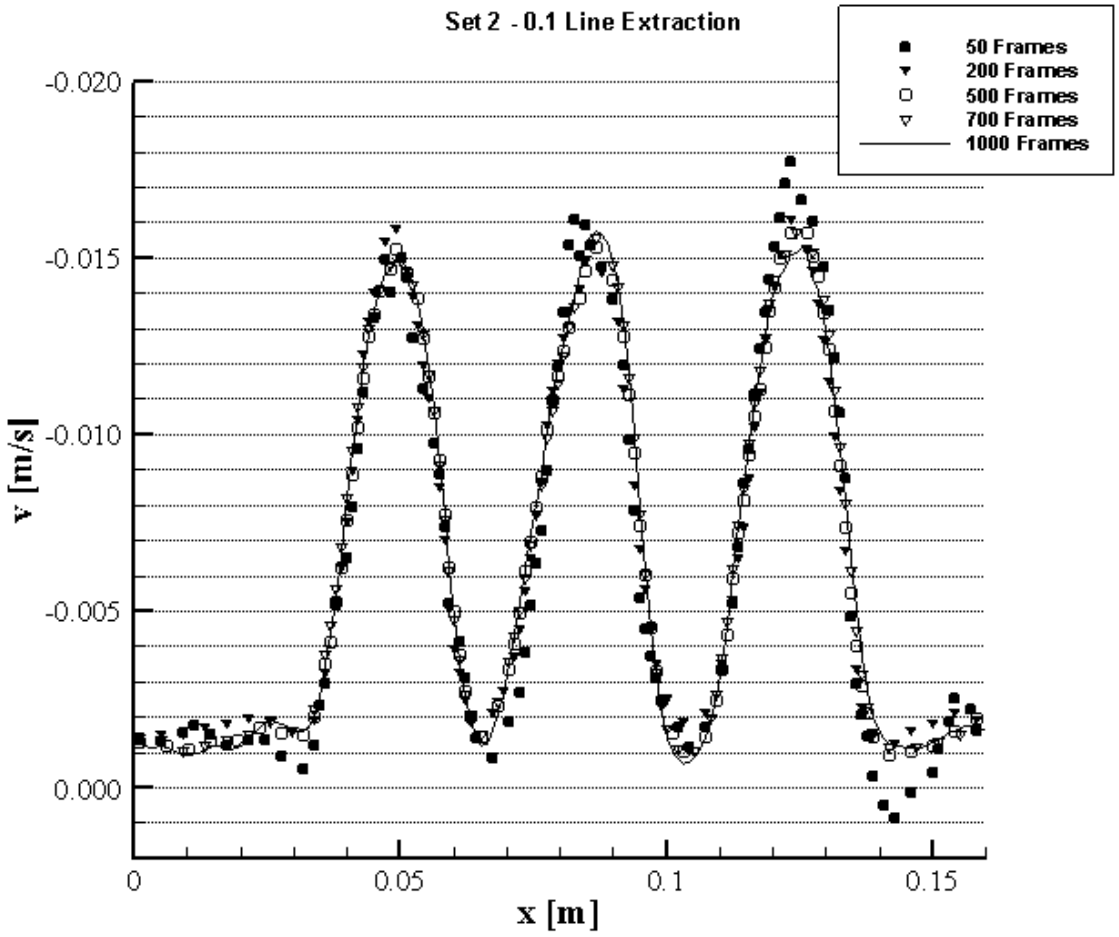

Figure 4-10: Sensitivity analysis for set 2 - 0.1m line

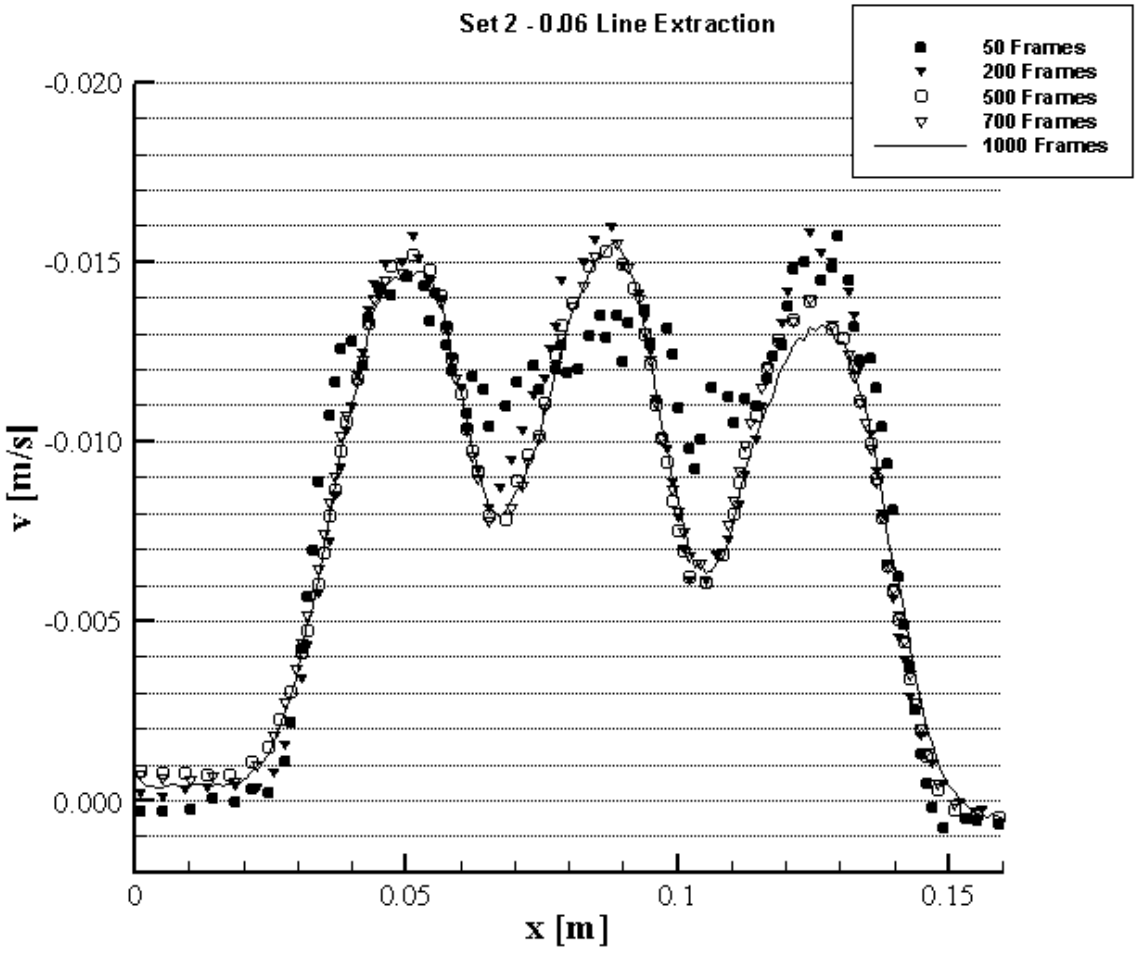

Figure 4-11: Sensitivity analysis for set 2 - 0.06 m line

Repeatability is important for testing to be valid. Test results in general will never perfectly match. For this test facility repeatability error could be due to multiple issues; the water being pumped through the cooling jacket may be colder one test than the other, or the ambient temperature may vary. As long as the tests are close the results can be compared. However the larger the deviation between the tests the lower the accuracy of the benchmark values the tests would produce. To evaluate the repeatability,

RMS was calculated for the Y-velocity line extraction at 0.1 m for all three tests. This value is representative of the error. This was then plotted with the velocity as the error bar in Figure 4-13. The error at the peaks range from 9-12% which isn't optimal but sufficient to state the tests are repeatable. From the sensitivity analysis set 1 has shown to have more error due to the poor particle density. With more tests the repeatability error should decrease.

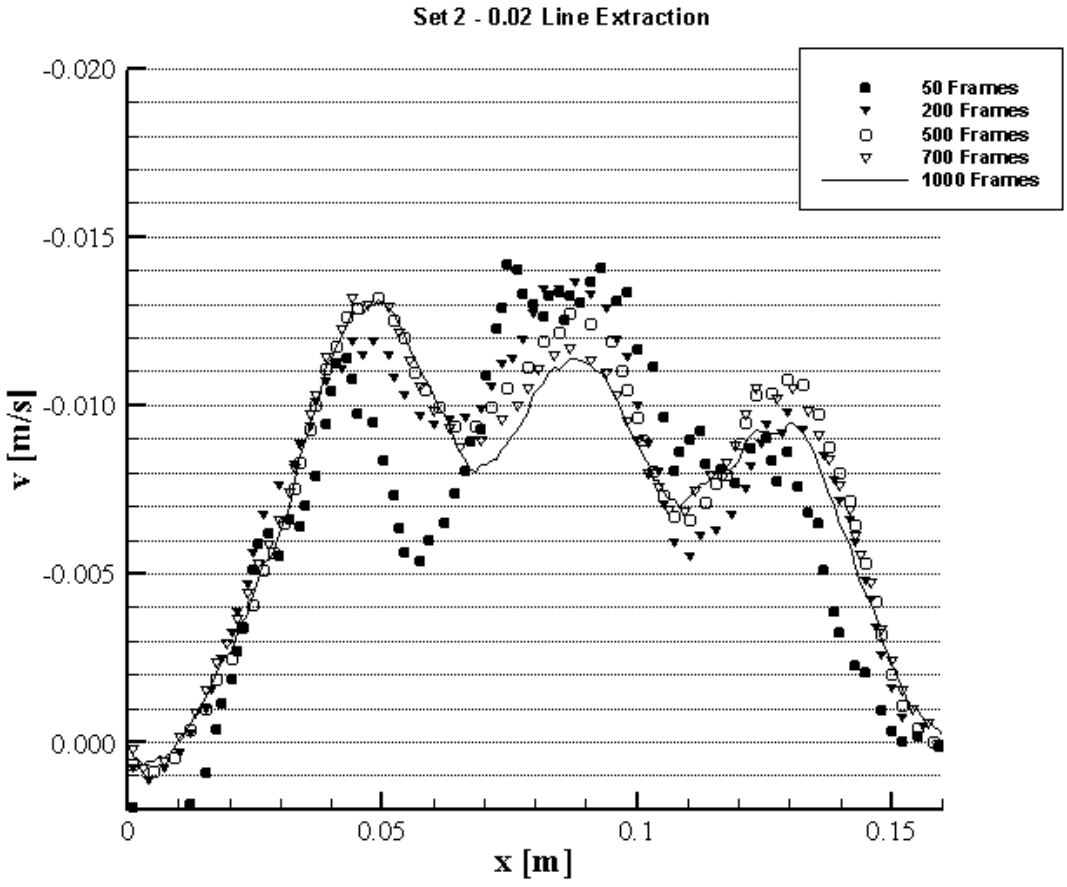

Figure 4-12: Sensitivity analysis for set 2 - 0.02 m line

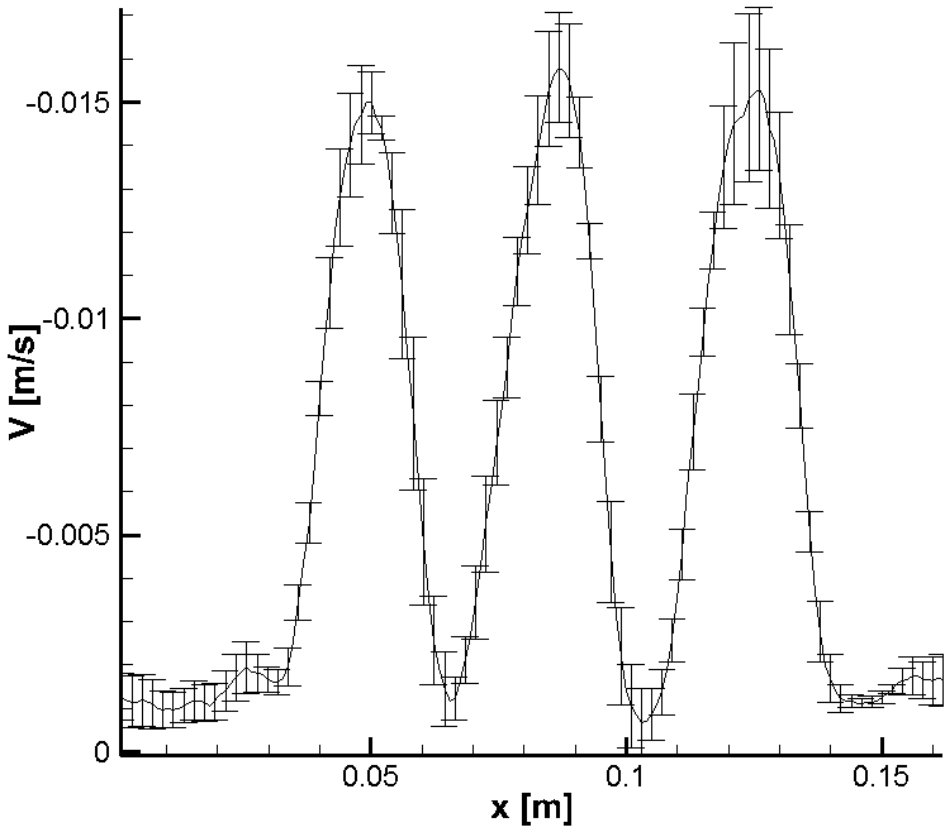

Figure 4-13: Repeatability

The pipe flow in the core piping is laminar with a Reynolds number around 200. However when it enters the upper plenum and the jets interact the fluid likely turns turbulent, but how turbulent. Turbulence intensity (TI) is a useful indicator for predicting how turbulent the flow is. Turbulence intensity is the standard deviation of the velocity fluctuation divided by the average velocity over the same time period. To test this when the line data was extracted the standard deviation of the velocity fluctuations was also calculated, shown in Figure 4-14. At the peak velocities the deviation was approximately 40% of the averaged velocity, so TI=0.4. This means the flow becomes turbulent despite

being laminar in the core piping. As the jets continue to mix the TI increases to 46% at 11 cm from the outlet.

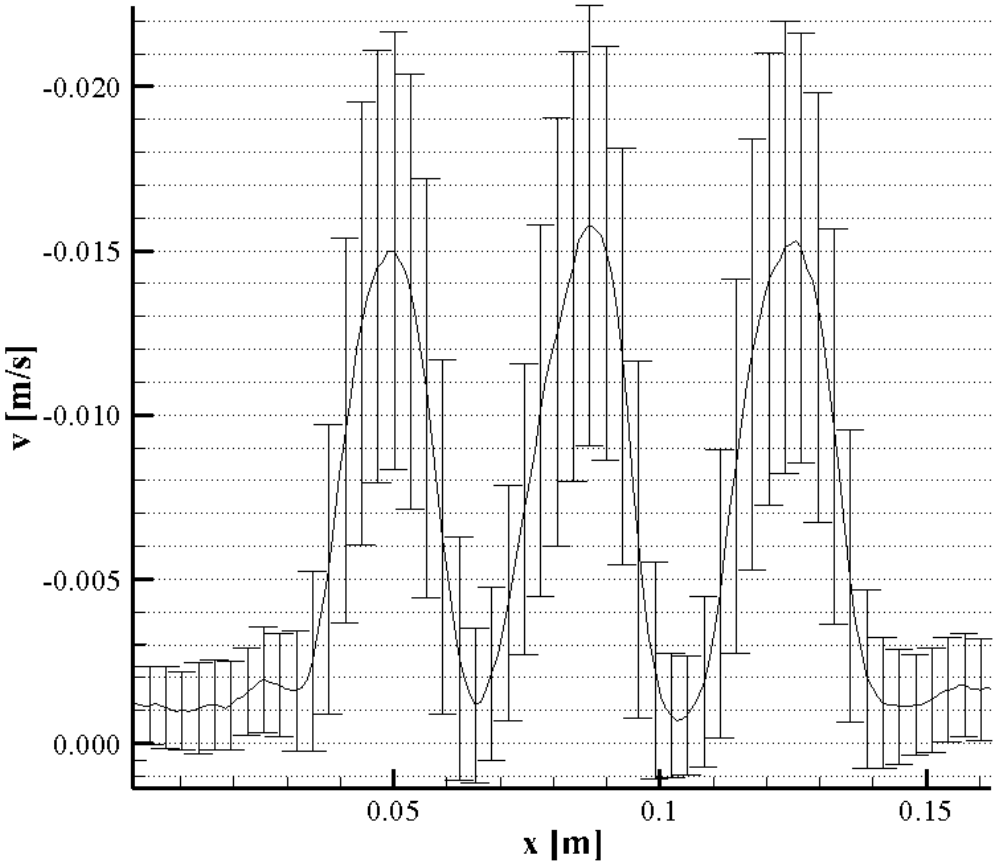

Figure 4-14: Standard deviation of turbulent velocity fluctuations for set 2 at Y=0.1m.

In order for the PIV results to be trusted they must be validated. This can be done both by calculation and experimentally. The flow rate of a single pipe may be calculated using,

$$Q = \dot{m} c_p \Delta T \rightarrow \dot{m} = \frac{Q}{c_p \Delta T} \tag{4.2}$$

In this equation Q is the heat input (Watts), $\dot{m}$ is the mass flow rate (kg/s), c_p is the specific heat (J/K), and ΔT is the temperature rise in the core piping (K). The accuracy of this value is determined by the accuracy of the thermocouples. The ultrasonic flow rate is the averaged flow rate from the flowmeter over the time the images were being taken, and then divided by five to account for the flow rate of a single pipe. For the PIV flow rate the velocity data at the outlet for all three pipes in the velocity contour was extracted. Then the mean of these averages was used as the average velocity for the outlets of the pipes. Using the average velocity for the outlets of the pipes flow rate could be determined by the equation $\dot{m} = v \rho A$.Because the velocity immediately above the outlet in the PIV velocity contour is false, the data was extracted slightly above the outlet once the flow profile was fully developed. The error was calculated for all three methods to determine if the measurements were within the error range of each other. As shown in Figure 4-15 these values match each other closely, the largest difference is between the calculated flow rate and the PIV flow rate in test one, which differ by 8%,however test 1 has shown to possibly be unreliable. Overall this is sufficient to validate the PIV results.

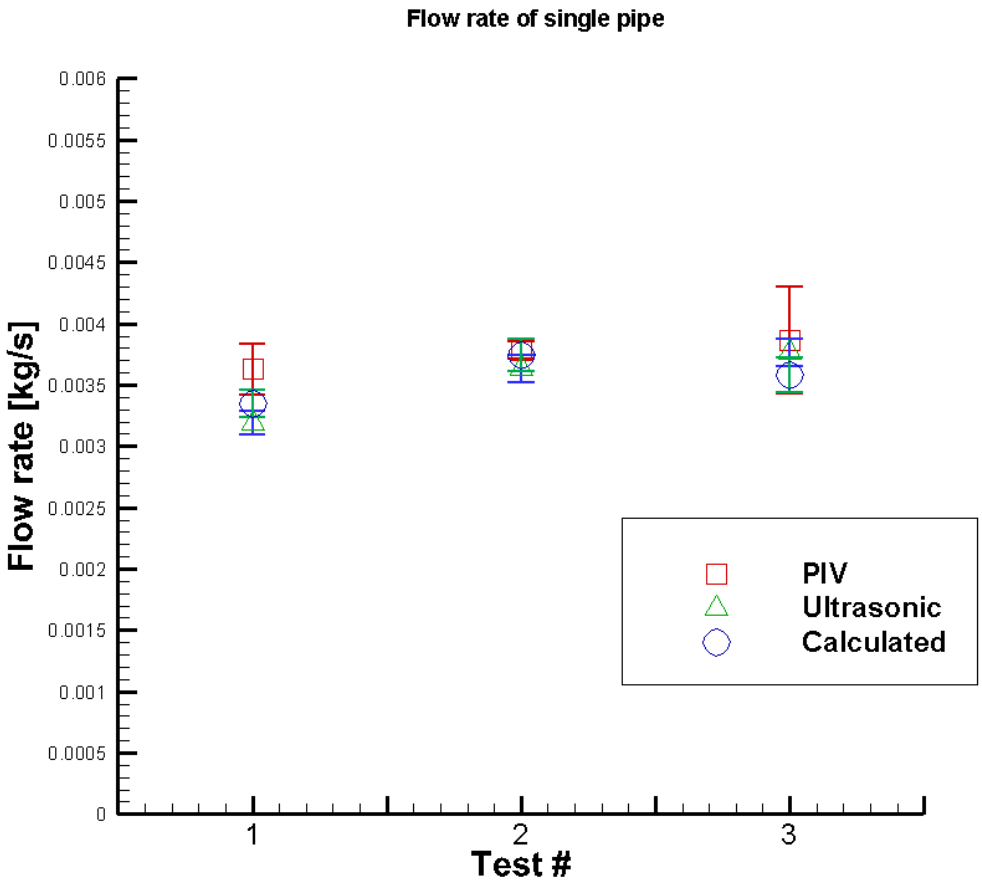

Figure 4-15: Flow rates for single pipe with different methods

For the ultrasonic flowmeter the error was matched to the electromagnetic flowmeter, which is 3%. The PIV error was calculated from the standard deviation of the average velocity of the three jets. The error for the calculated flow rate comes from the error in the thermocouples. The error caused by the thermocouples in equation 4.2 may be calculated using equations 4.3 and 4.4.

$$\xi_{\dot{m}} = \sqrt{\left(\frac{d\dot{m}}{dT_i}\right)^2 \sigma_{Ti}{}^2 + \left(\frac{d\dot{m}}{dT_o}\right)^2 \sigma_{To}{}^2} \tag{4.3}$$

$$\xi_{\dot{m}} = \sqrt{\left(\frac{Q}{c_p}\frac{1}{(T_o - T_i)^2}\right)^2 0.5^2 + \left(\frac{Q}{c_p}\frac{1}{(T_o - T_i)^2}\right)^2 0.5^2} \quad (4.4)$$

4.4 Computer Fluid Dynamics Modeling

The endgoal of this experiment is to supply benchmark data that may be used to validate CFD models. To properly design the facility and run tests that would sufficiently produce benchmark data an understanding of CFD is necessary. To accomplish this a Star-ccm+ CFD model was generated that models the fluid region of the experimental test facility. Star-ccm+ uses three continuity equations: mass, momentum, and energy. These equations are evaluated using finite volume discretization. The equations may be solved simulanesouly with the coupled energy model, or separately with the segregated energy model. A mesh of the experimental facility has been developed using Star-CCM+ in Figure 4-16. The mesh consists of three regions. The main gas reactor fluid region, the cooling jacket fluid region, and a steel region between them. Interfaces were created for both fluid reagions and the steel section that allows for heat transfer from one region to another. For all regions a polyhedral mesher was used with a prism layer mesher that generates cells a thin layer of cells at the boundaries of the regions. A denser mesh was used for the gas reactor region, particularly in the upper plenum. The final mesh contains approximately 2.5 million cells.

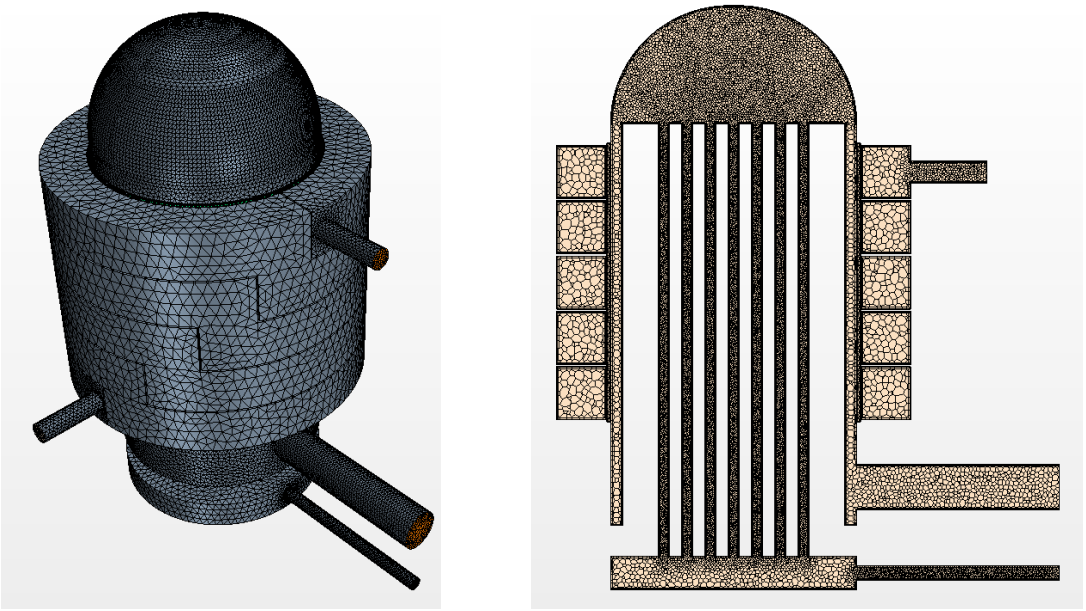

Figure 4-16: Test facility CFD model

For this study the segregated energy model was chosen so the energy equation would be solved separately. For the main loop a laminar model was chosen as the flow rate for the experiment is slow. As this study has shown the flow in the upper plenum is actually turbulent, but once the turbulent fluctuations are averaged out and the statistically steady from the PIV analysis may be similar to the laminar results for cfd modeing. For natural convection the Boussinesq Approximation is applicable, however for a model of this scale applying such an approximation as the driving force for the fluid is challenging and it usually causes the residuals to quickly diverge. Addtionally a study has shown that using the incompressible flow assumption in high heat flux situations may lead to misrepresentative results [26]. Instead boundary conditions were derived from the experimental set up to perform a forced convection simulation with a constant density model. The inlet has a mass flow boundary condition that was taken

from one of the pre-calibration ultrasonic flowmeter measurements. A total of 10 kW heat input was evenly distributed on the surfaces of the 25 pipes. The outlet condition was a pressure outlet set to zero.

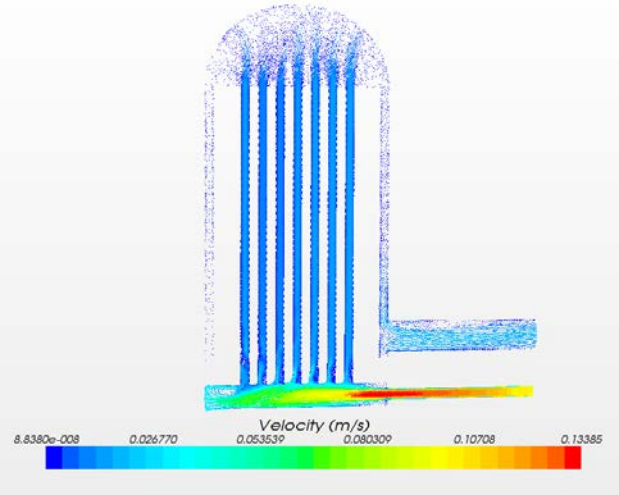

Figure 4-17: Velocity field of gas reactor fluid region

The cooling jacket inlet was set to 10.5 GPM. The physics models were the same as the gas reactor fluid region except a k-epsilon turbulence model was chosen instead of laminar. As stated before the experimental design allows the pipe orientation in resepct to the inlet to have either three or seven pipes aligned with the inlet. This determines the number of pipes the symmetric plane would have. The orientation for this simulation is the opposite of the experimental set up which has seven pipes in the symmetric plane. With these conditions the simulation was run.

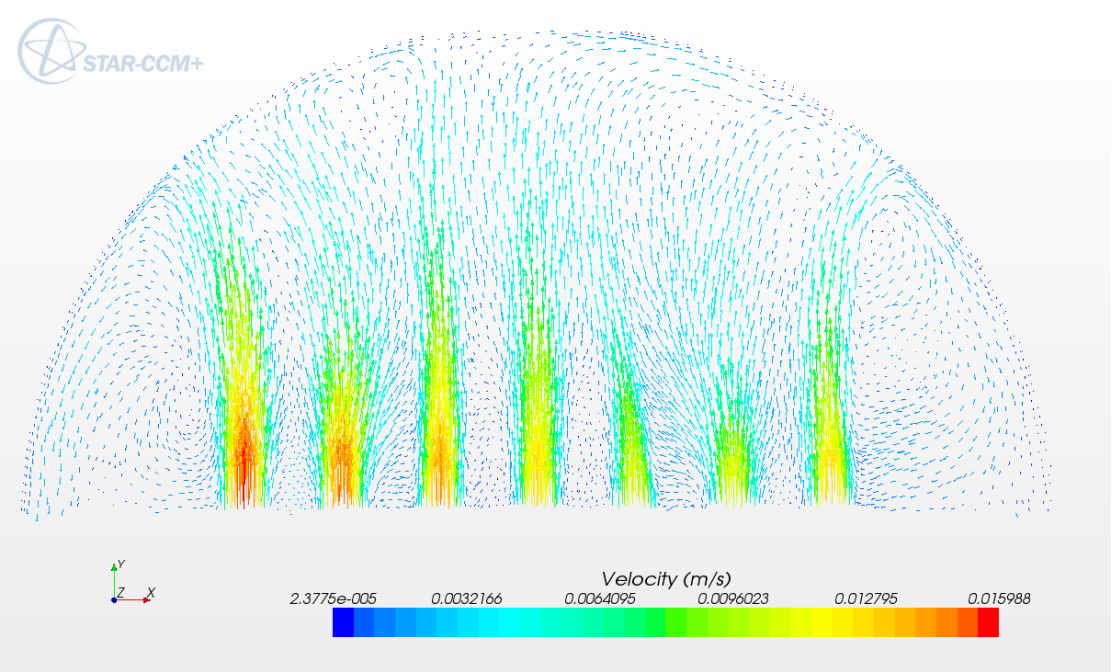

Figure 4-18: Non-symmetric cross section of upper plenum

Figure 4-17 shows the velocity cross section of the gas reactor fluid region. It shows the velocity profile in the lower plenum, however since the inlet has a velocity 25 times greater than the individual core piping, the scaling doesn't reveal much about the velocity behavior in the rest of the model. Figure 4-18 shows the velocity profile of the non-symmetric cross section of the upper plenum. Since the flow is laminar there is little jet to jet interaction, although some eddies are generated between farther from the inlets. Figure 4-19 shows the symmetric plane of the upper plenum. Apparently the flow isn't perfectly symmetric as the flow in the right jet is stronger than that of the left, suggesting

that even though the mass and momentum equations converged the simulation may be misrepresentative of the actual flow profile in the experimental facility.

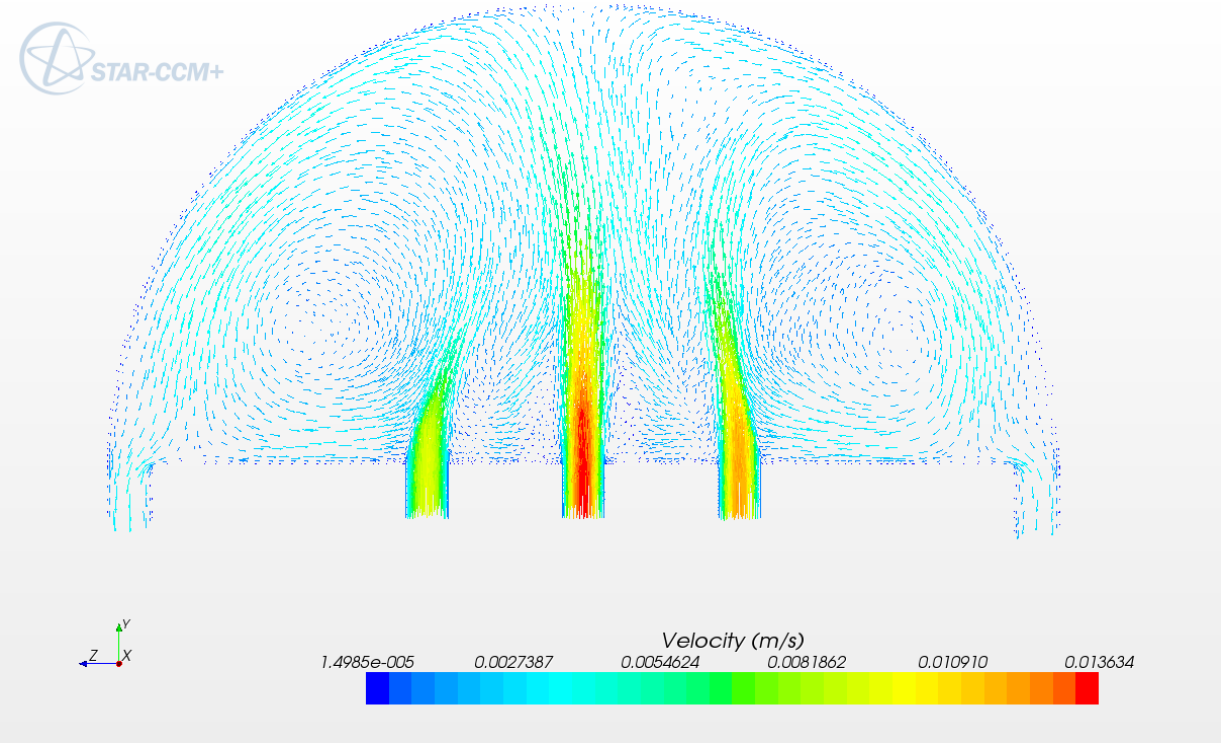

Figure 4-19: Symmetric cross section of upper plenum

The energy equation did not converge. The residuals fluctuated around 0.01. The under-relaxation factor for the fluid was lowered to 0.1 however this did not do much to reduce the energy residual. The model is large and rather ambitious. To properly simulate a much finer mesh is likely needed, perhaps at least five times the cell count. Another option would be to only model the upper plenum and just use boundary conditions from the experimental facility to the pipe inlet velocity profile. If this does

not work a half model upper plenum with a symmetric boundary condition could be modeled. Further research into modeling natural convection is necessary to determine how to model it.

5 CONCLUSION AND FUTURE WORK

5.1 Conclusion

Currently there is no benchmark experimental data to validate CFD codes modeling the upper plenum of a VHTR after a PCC accident scenario. The goal of this study was to build an experimental facility that could fill this deficiency of data. To accomplish this a $1/16^{th}$ scaled geometry from Idaho National Laboratories was incorporated into a design that can model a VHTR under a PCC condition, and allows for proper data acquisition for validation and obtaining benchmark data. The design was then approved and forwarded to the fabricators. Once the parts were machined the experimental facility was then assembled. Problems such as leaks and burnt out heating tapes were encountered, and corrective action was taken until the facility was functional again.

The testing procedure was explained and particle images for PIV analysis as well as other corresponding data that could be used for analyzing a statistically steady state condition for partial operation. Three separate steady state tests were processed using PIVlab to generate the vector fields and exported them to text files. A Matlab code was used to average the varying batch sizes of text files. A sensitivity analysis was performed to determine the number of image pairs needed for the PIV system to obtain benchmarking data. When the flow is close to the jet outlet 500 frames are sufficient, however once the jets start mixing at about twelve centimeters from the outlet at least 700 image pairs are required. This is due to the turbulent behavior of the fluid. After taking the standard deviation of the fluid velocity for 1000 image pairs the turbulence

intensity of the jets was approximately 0.4 or 40% of the flow velocity, which increased to 46% at 13 cm from the pipe outlet. Additionaly recirculation between the jets occurred until the merging point 3 cm from the pipe outlet. The converging point was never reached. Next the repeatability of tests was validated by comparing the standard deviation of the averaged velocity fields between the tests. The relative standard deviation was approximately 10% at the jet peaks but may be reduced if more tests are run. Next the flow rate of a single pipe was measured with three methods: ultrasonic flowmeter, PIV velocity extraction, and calculated using the temperature rise of the core piping. The flow rates matched and will all lie within their error boundary.

A CFD model and simulation was tested to provide insight on proper methods of modeling the experimental facility. Applying the Boussinesq approximation for natural convection to a full scale model of the test facility is unrealistic. A forced convection simulation may be possible if a very large number of cells were used. An easier solution would be to model only the upper plenum and assigning the velocity profiles measured with PIV to the pipe outlets in the upper plenum of the CFD model.

The test facility constructed in this study can produce reliable particle imaging for PIV analysis for natural convective flow. With this benchmark data may be produced for CFD code validation. This includes data modeling the mixing of a select number of natural convective jets, as well as modeling a VHTR during a PCC scenario.

5.2 Future Work

First more tests should be run to further evaluate the repeatability. Next the images collected should be processed with different codes, primarily with Particle

Tracking Velocimetry. The PIV results were validated using experimental data, but PTV may prove more effective at processing the images than PIV, and if not it would still be beneficial to further validate the PIV results. Also more statistically steady state tests may be run to test the repeatability of the experiment. Next a full scale test may be run with all 25 pipes operating.

Planar laser induced fluorescence (PLIF) is a process used to record the temperature field of a 2-d planar cross section that can be performed simultaneously with PIV. This has great applications for this test facility and can be used to provide benchmark data for CFD code validations. Also more advanced methods exist for measuring the velocity field. Stereoscopic PIV uses multiple cameras to measure all three velocity components of the planar cross section illuminated by the light sheet. And beyond that is topographic mapping that can measure the velocity behavior of a 3D volume.

CFD simulations need to be run and compared to the results of this experiment. This includes the results from this study, as well as the full scale tests. This will determine the quality of benchmark data that the test facility can produce.

The novelty of this test facility is that it has the flexibility to be modified to test different scenarios and configurations the user chooses. It has applications beyond the scope of this study, and will continue to be beneficial to fluid modeling.

REFERENCES

1. Energy, U.S.D.o., *Primary Energy Overview*. 2014, U.S. Energy Information Administration: Washington DC.
2. Westinghouse Nuclear. *AP1000*. 2007; Available from: http://www.westinghousenuclear.com/docs/AP1000_brochure.pdf.
3. Doug Chapin, S.K., Jim Nestell, *The Very High Temperature Reactor: A Technical Summary*. 2004: MPR Associates Inc. Alexandria, VA.
4. Birkhofer, A., *Advanced Power Reactors with Improved Safety Characteristics.* Applied radiation and isotopes, 1995. **46**(6): p. 701-706.
5. MacDonald, P.E., P. Bayless, H. Gougar, R. Moore, A. Ougouag, et al. *The next generation nuclear plant–insights gained from the INEEL point design studies*. in *INEEL, INEEL/CON-04-01563*. 2004. Pittsburgh, PA.
6. Khamis, I. *Nuclear power plants can produce hydrogen to fuel the "hydrogen economy"*, in *ACS Press Conference*. 2012. San Diego, California: American Chemical Society
7. Ehresman, T., *Very High Temperature Reactor [VHTR]*. 2014; Idaho National Laboratory, Idaho Falls, Idaho.
8. Reyes Jr, J., J. Groome, B. Woods, B. Jackson, and T. Marshall, *Scaling Analysis for the High Temperature Gas Reactor Test Section (GRTS).* Nuclear Engineering and Design, 2010. **240**(2): p. 397-404.
9. Haque, H., W. Feltes, and G. Brinkmann, *Thermal Response of a Modular High Temperature Reactor During Passive Cooldown under Pressurized and*

Depressurized Conditions. Nuclear Engineering and Design, 2006. **236**(5–6): p. 475-484.

10. Schürenkrämer, M., *Theoretische und experimentelle Untersuchungen der Naturkonvektion im Kern des Kugelhaufen-Hochtemperaturreaktors*. 1984, Zentralbibliothek d. Kernforschungsanlage.
11. Tung, Y.-H. and R.W. Johnson. *CFD calculations of natural circulation in a high temperature gas reactor following pressurized circulator shutdown*. in *ASME 2011 International Mechanical Engineering Congress and Exposition*. 2011. Denver, Colorado, USA: American Society of Mechanical Engineers.
12. Tauveron, N., *Thermal Fluctuations in the Lower Plenum of a High Temperature Reactor.* Nuclear engineering and design, 2003. **222**(2): p. 125-137.
13. Barre, F. and M. Bernard, *The CATHARE Code Strategy and Assessment.* Nuclear engineering and design, 1990. **124**(3): p. 257-284.
14. Chang, H.O., C. Davis, and R. Moore, *Development of Safety Analysis Codes and Experimental Validation for a Very High Temperature Gas-Cooled Reactor*. 2004, Idaho National Laboratory, Idaho Falls, Idaho.
15. McCreery, G.E., K.G. Condie, and R.R. Schultz. *Scaled experimental modeling of VHTR plenum flows*. in *Proceedings of the 15th International Conference on Nuclear Engineering (ICONE 15), Nagoya, Japan*. 2007.
16. Tritton, D.J., *Physical Fluid Dynamics*. 1977, New York: Van Nostrand Reinhold.

17. McCreery, G.E. and K.G. Condie, *Experimental modeling of VHTR plenum flows during normal operation and pressurized conduction cooldown*. 2006, INL/EXT-06-11760, Idaho National Laboratory, Idaho Falls, Idaho.

18. Aldridge, R.J., *Scaling study of the depressurized conduction cooldown event in the high temperature test facility using RELAP5-3D/ATHENA. (Doctoral dissertation),* in *Nuclear Engineering*. 2013, Oregon State University: Corvallis, OR.

19. King, B., *Natural Circulation Scaling of a Pressurized Conduction Cooldown Event in the Upper Plenum of the Modular High Temperature Gas Reactor. (Master's thesis),* in *Nuclear Engineering*. 2012, Oregon State University. p. 78.

20. Jahanmiri, M., *Particle Image Velocimetry: Fundamentals and Its Applications*. 2011, Chalmers University of Technology, Goeteborg, Sweden.

21. Keane, R.D. and R.J. Adrian, *Theory of Cross-Correlation Analysis of PIV Images.* Applied scientific research, 1992. **49**(3): p. 191-215.

22. Bastiaans, R.J., *Cross-correlation PIV; theory, implementation and accuracy*. 2000: Eindhoven University of Technology, Einhoven, Netherlands, Faculty of Mechanical Engineering.

23. Meinhart, C.D., S.T. Wereley, and J.G. Santiago, *A PIV Algorithm for Estimating Time-Averaged Velocity Fields.* Journal of Fluids Engineering, 2000. **122**(2): p. 285-289.

24. Nogueira, J., A. Lecuona, and P. Rodriguez, *Data Validation, False Vectors Correction and Derived Magnitudes Calculation on PIV Data.* Measurement Science and Technology, 1997. **8**(12): p. 1493.

25. Fukushima, C., L. Aanen, and J. Westerweel, *Investigation of the mixing process in an axisymmetric turbulent jet using PIV and LIF*, in *Laser Techniques for Fluid Mechanics*. 2002, Springer Berlin Heidelberg, Germany. p. 339-356.

26. Martineau, R.C., R.A. Berry, A. Esteve, K.D. Hamman, D.A. Knoll, et al., *Comparative Analysis of natural convection flows simulated by both the conservation and incompressible forms of the Navier-Stokes equations in a differentially heated square cavity*. 2009, Idaho National Laboratory, Idaho Falls, Idaho.

APPENDIX A

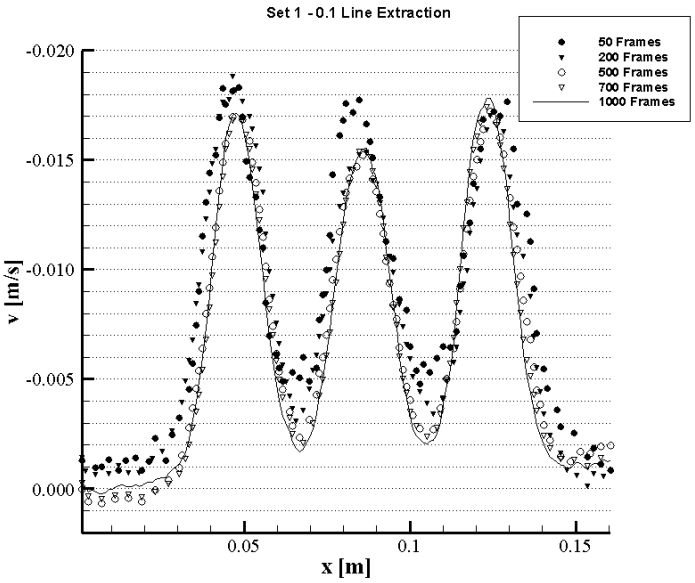

Figure A-1: Sensitivity Analysis for set 1 - 0.1m line extraction

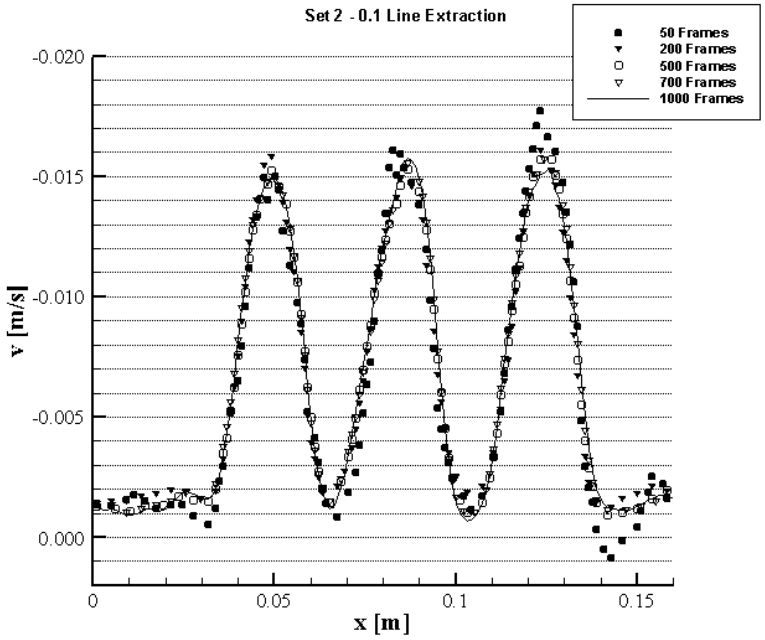

Figure A-2: Sensitivity analysis for set 2 – 0.1 m line extraction

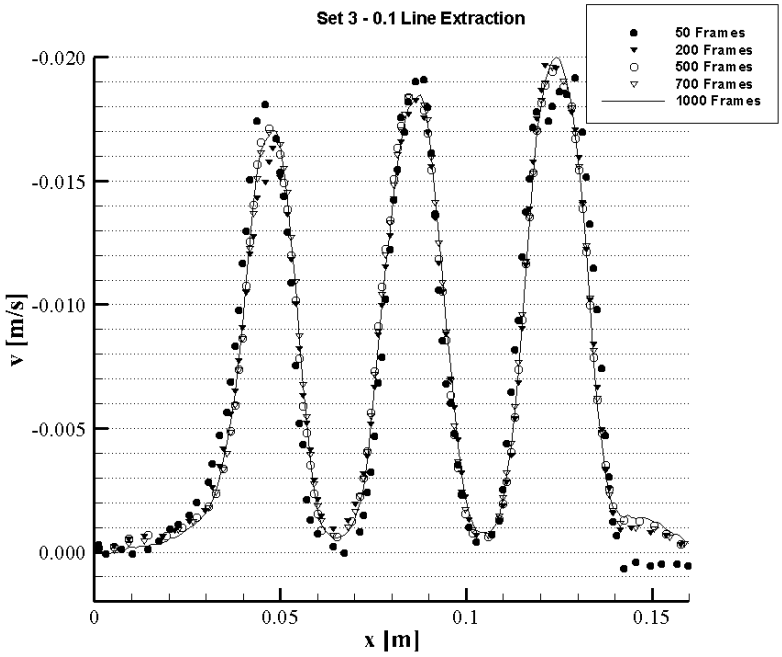

Figure A-3: Sensitivity analysis for set 3 – 0.1 m line extraction

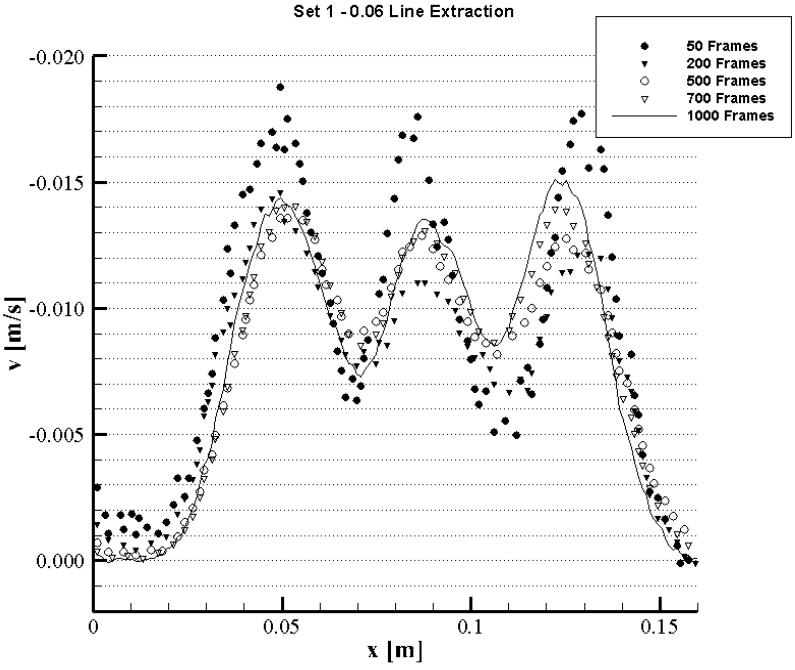

Figure A-4: Sensitivity analysis for set 1 – 0.06 m line extraction

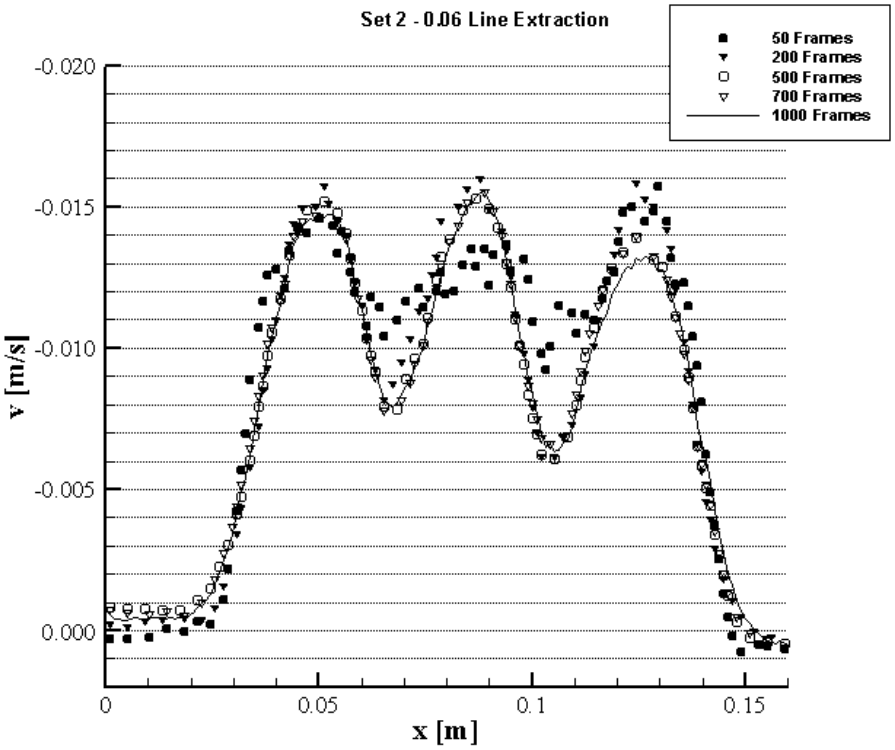

Figure A-5: Sensitivity analysis for set 2 – 0.06 m line extraction

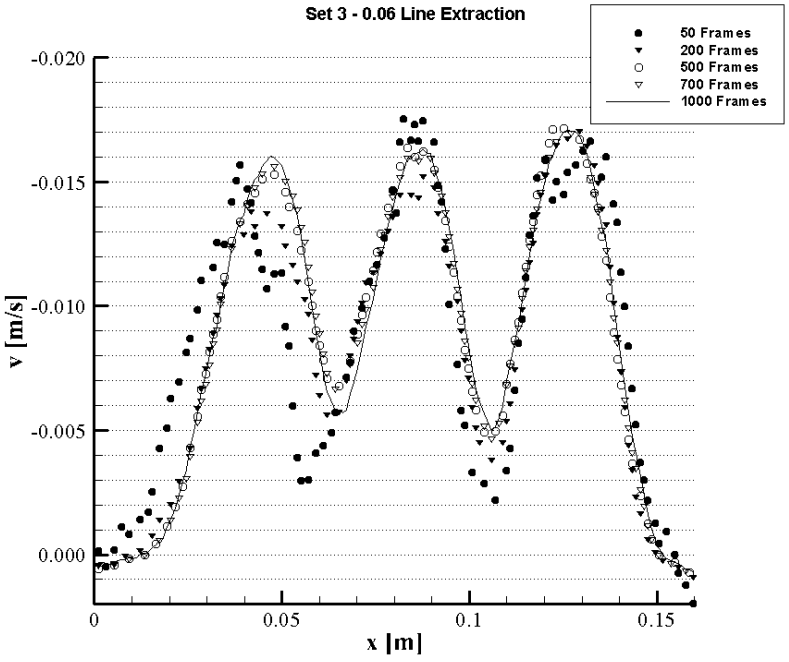

Figure A-6: Sensitivity analysis for set 3 – 0.06 m line extraction

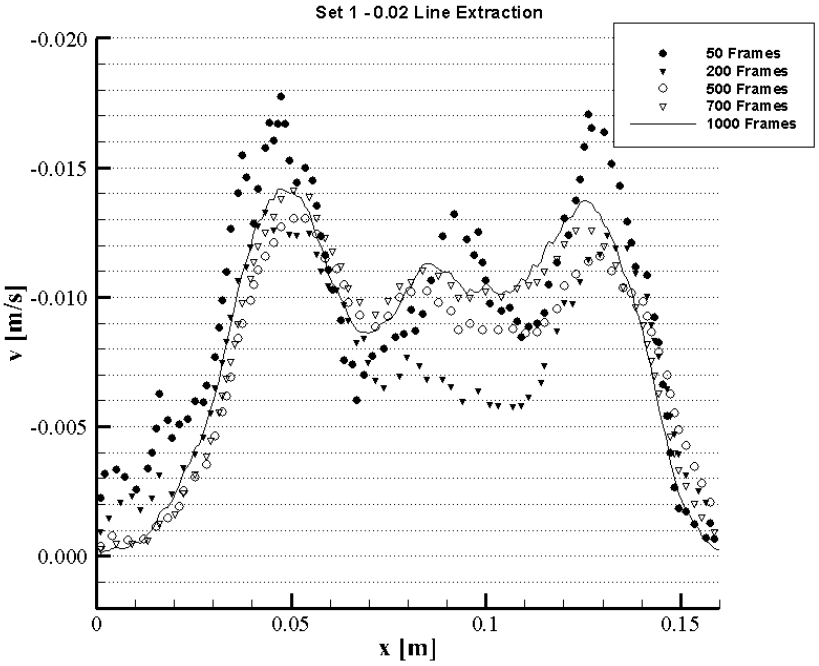

Figure A-7: Sensitivity analysis for set 1 – 0.02 m line extraction

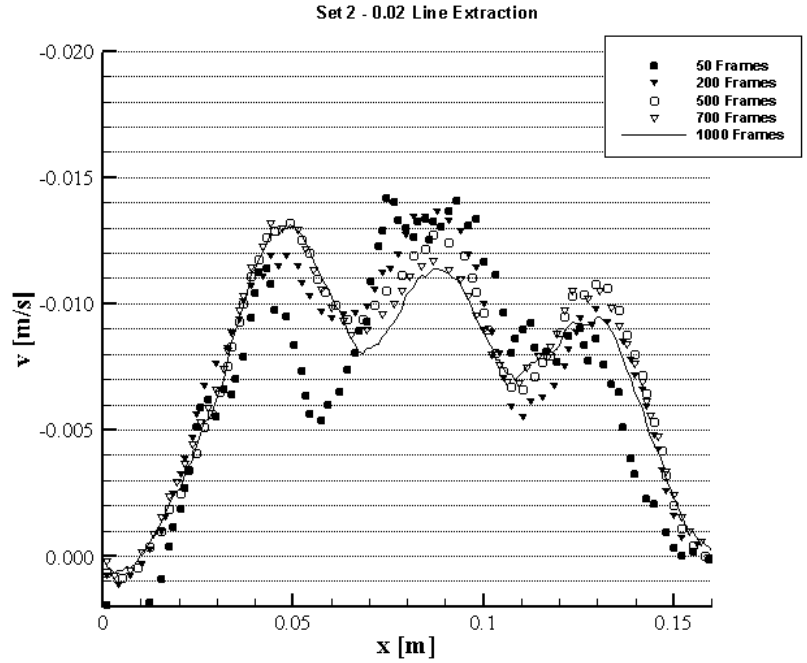

Figure A-8: Sensitivity analysis for set 2 – 0.02 m line extraction

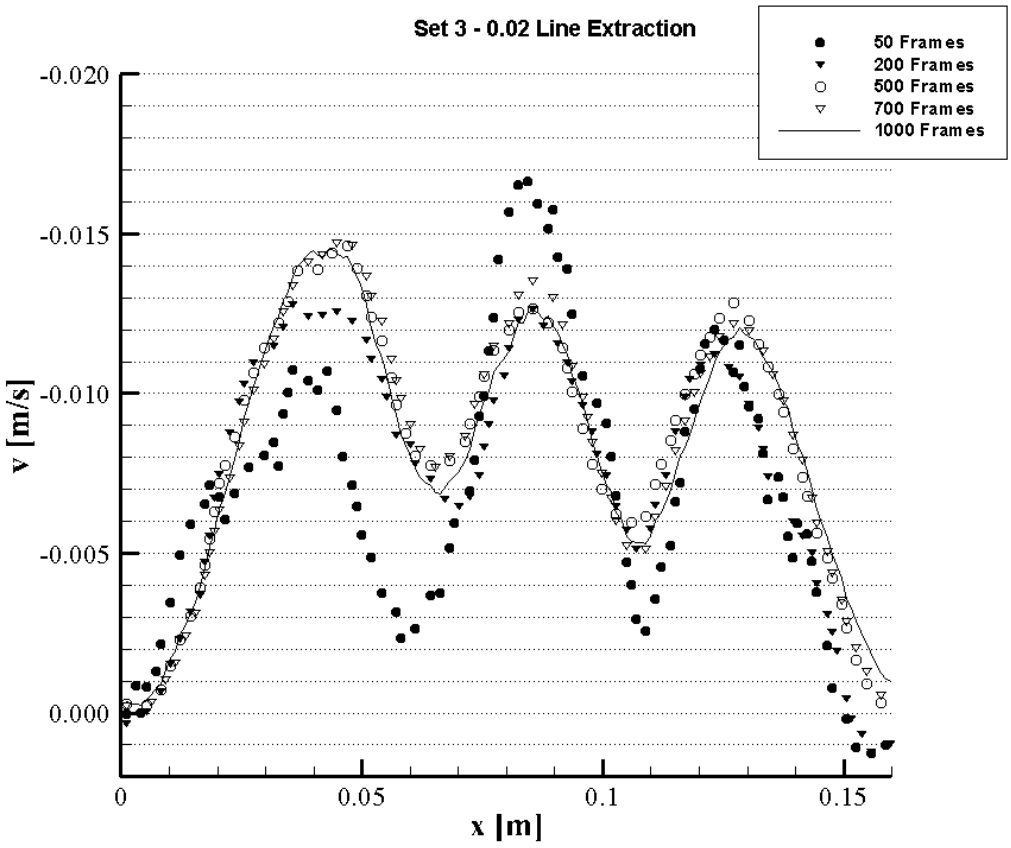

Figure A-9: Sensitivity analysis for set 3 – 0.02 m line extraction